

1 ~~Long-range transported pollution from the Middle East and its~~
2 ~~impact on carbonaceous aerosol sources over Cyprus.~~ Ambient
3 carbonaceous aerosol levels in Cyprus and the role of pollution
4 transport from the Middle East.

5 Alikı Christodoulou^{1,2}, Iasonas Stavroulas^{1,3}, Mihalis Vrekoussis^{1,4,5}, Maximillien Desservettaz¹, Michael Pikridas¹,
6 Elie Bimenyimana¹, Jonilda Kushta¹, Matic Ivančič⁶, Martin Rigler⁶, Philippe Goloub⁷, Konstantina Oikonomou¹,
7 Roland Sarda-Estève⁸, Chrysanthos Savvides⁹, Charbel Afif^{1,10}, Nikos Mihalopoulos^{1,3}, Stéphane Sauvage² and
8 Jean Sciare¹

10 ¹Climate and Atmosphere Research Center (CARE-C), the Cyprus Institute, Nicosia, 2121, Cyprus

11 ²IMT Nord Europe, Institut Mines-Télécom, Univ. Lille, Centre for Energy and Environment, 59000 Lille, France

12 ³Institute for Environmental Research and Sustainable Development, National Observatory of Athens, Athens, Greece

13 ⁴University of Bremen, Institute of Environmental Physics and Remote Sensing (IUP), University of Bremen, Germany

14 ⁵Center of Marine Environmental Sciences (MARUM), University of Bremen, Germany

15 ⁶Aerosol d.o.o., Research & Development Department, Kamniška 39a, SI-1000 Ljubljana, Slovenia

16 ⁷University of Lille, CNRS, LOA – Laboratoire d’Optique Atmosphérique, Lille, 59000, France

17 ⁸Laboratoire des Sciences du Climat et de l’Environnement (LSCE), CNRS-CEA-UVSQ, Gif-sur-Yvette, France

18 ⁹Ministry of Labour and Social Insurance, Department of Labour Inspection (DLI), Nicosia, Cyprus

19 ¹⁰Emissions, Measurements, and Modeling of the Atmosphere (EMMA) Laboratory, CAR, Faculty of Sciences, Saint Joseph

20 University, Beirut, Lebanon

22 *Correspondence to:* Alikı Christodoulou (a.christodoulou@cyi.ac.cy) and Jean Sciare (j.sciare@cyi.ac.cy)

23 **Abstract.** The geographical origin and source apportionment of submicron carbonaceous aerosols (organic aerosols, OA, and
24 black carbon, BC) have been investigated here for the first time ~~by means of deploying~~ high-time resolution measurements at
25 an urban background site of Nicosia, the capital city of Cyprus, in the Eastern Mediterranean. This study covers a half-year
26 period, encompassing both the cold and warm periods with continuous observations of the physical and chemical properties
27 of PM₁ performed with an Aerosol Chemical Speciation monitor (ACSM), an Aethalometer, accompanied by a suite of various
28 ancillary off and on-line measurements. Carbonaceous aerosols were dominant during both seasons (cold and warm periods),
29 with a ~~respective~~ contribution of 57% and 48% to PM₁, respectively, and exhibited recurrent intense night-time peaks (>20-
30 30 μg m⁻³) during the cold period associated with local domestic heating. ~~The F~~findings of this study show that high
31 concentrations of sulfate (close to 3 μg m⁻³) were continuously recorded, standing among the highest ever reported for Europe
32 and originating from the Middle East region.

33 Source apportionment of the OA and BC fractions was performed using the Positive Matrix Factorization (PMF) approach and
34 the combination of two models (aethalometer model and multilinear regression), respectively. Our study revealed elevated
35 hydrocarbon-like organic aerosol (HOA) concentrations in Nicosia (among the highest reported for a European urban
36 background site), originating from a mixture of local and regional fossil-fuel combustion sources. Although air masses from
37 the Middle East had a low occurrence and were observed mostly during the cold period, they were shown to strongly affect
38 the mean concentrations levels of BC and OA in Nicosia during both seasons. Overall, the present study brings to our attention
39 the need to further characterize primary and secondary carbonaceous aerosols in the Middle East; an undersampled region
40 characterized by continuously increasing fossil fuel (oil and gas) emissions and extreme environmental conditions, which can
41 contribute to photochemical aging.

42 1. Introduction

43 At the crossroads of three continents (Europe, Africa, Asia), the Eastern Mediterranean and Middle East (EMME) region faces
44 many challenges, such as rapid population growth – with its currently 400 million inhabitants – as well as political and socio-
45 economic instabilities. Environmental conditions in the region are exceptional, with the two largest deserts worldwide (Sahara
46 ~~and~~; Arabian) being among the most water scarce ecosystems on the planet (Terink et al., 2013). Climate change in this region
47 is extraordinarily rapid; summer temperatures, in particular, are increasing by more than twice the global mean rate (Lelieveld
48 et al., 2014), with significant impacts, especially in urban areas (Mouzourides et al., 2015). While aerosol mass loadings over
49 the EMME are dominated by desert dust, concentrations of fine particles due to anthropogenic emissions are also high (Basart
50 et al., 2009) and will likely increase with continued population growth (Pozzer et al., 2012), making anthropogenic pollution
51 in the area a leading health risk and an important climate forcer (Osipov et al., 2022).

52 Based on modelling studies, it has been also concluded that the EMME is characterized by highly favourable conditions for
53 photochemical smog and ozone (O₃) formation leading to air quality standards being drastically exceeded (Lelieveld et al.,
54 2014; Zanis et al., 2014). These enhanced concentrations of fine particulates and ozone have major human health implications,
55 contributing to premature mortality (Giannadaki et al., 2014; Lelieveld et al., 2015), which may be further exacerbated by the
56 effects of heatwaves occurring during summer within the EMME region (Zittis et al., 2022).

57 Although data ~~derived~~ from satellite observations of NO₂ and SO₂ has revealed strong air pollution trends in the Middle East
58 since 2010 (Lelieveld et al., 2015a), many pollution sources are still missing in emission inventories (Mclinden et al., 2016).
59 Thus, there is a current lack of a regional approach to characterize air pollution, with in-situ observation being insufficient,
60 unavailable, or of low quality (Kadygrov et al., 2015; Ricaud et al., 2018; Paris et al., 2021), limiting the possibility to reduce
61 uncertainties in regional emission inventories and implement efficient ~~abate~~ment strategies.

62 Significant efforts have been put forward in recent years to characterize the atmospheric composition in-situ over Cyprus, a
63 central location of the EMME region (e.g., Kleanthous et al., 2014; Debevec et al., 2017 and 2018; Pikridas et al., 2018; Dada
64 et al., 2020; Baalbaki et al., 2021; Vrekoussis et al., 2022). In-situ ground-based PM observations have clearly shown that
65 contributions of dust to PM₁₀ over Cyprus are among the highest for the entire Mediterranean basin (Querol et al., 2009; Pey
66 et al., 2013; Kleanthous et al., 2014; Pikridas et al., 2018; Achilleos et al., 2020), during dust storm events, leading to increased
67 hospitalization, particularly attributed to cardiovascular-related diseases (Middleton et al., 2008; Tsangari et al., 2016) and
68 short-term effects associated with daily mortality (Neophytou et al., 2013). These high levels of regional particulate matter are
69 responsible for exceedances in PM₁₀ EU limits in major Cypriot cities (Querol et al., 2009). Past studies on PM trends and
70 sources highlighted the important contribution of local (urban) emissions to PM₁₀ (Achilleos et al., 2014; Pikridas et al., 2018)
71 but also showed a predominant regional pattern for PM_{2.5} with ~~a~~ major contribution of sulphur-rich sources (Achilleos et al.,
72 2016). Based on 17 years of continuous observations of reactive gases in Cyprus, Vrekoussis et al., (2022) further confirmed
73 the major contribution of long-range transport (incl. Middle East) in the observed concentration levels of carbon monoxide
74 (CO) and sulphur dioxide (SO₂), two tracers of combustion sources.

75 Those studies have highlighted the unique location of Cyprus as a receptor site of major regional pollution hotspots, making
76 the island one of the most polluted EU member states in terms ~~of~~ PM and O₃ concentrations; the only one impacted by long-
77 range transport of poorly-regulated air pollutants originating from Middle East countries. However, ~~still~~ few studies are
78 currently available to assess the contribution of regional anthropogenic emissions to PM levels in Cyprus. The filter-based
79 chemical speciation study reported by Achilleos et al., (2016) is currently the most exhaustive one and was based on 24-h
80 integrated (PM_{2.5} and PM₁₀) filter samples collected every 3 days for a period of one year (2012) in four cities in Cyprus. This
81 study concluded that Cypriot cities, like many others in Europe, are characterized by a major contribution of regional sulphate
82 and local (urban) emissions from traffic and domestic heating biomass burning.

83 Herewith, a detailed description of submicron (<1µm, PM₁) chemical composition and the further source apportionment of BC
84 and OA is presented for the first time in Cyprus. State-of-the-art on-line instrumentation (e.g., Q-ACSM, Aethalometer) ~~were~~

85 was deployed ~~for the investigation to investigate of~~ the temporal variability of aerosol composition at a location representative
86 of the urban background pollution in the capital city of Nicosia. Source apportionment of submicron organic aerosols was
87 performed using the organic fragments of the ACSM and Positive Matrix Factorization (PMF). The consistency of these results
88 was assessed against the chemical analysis of parallel filter samples and on-line measurements of external tracers. This study
89 was extended to a 6-month duration in order to cover the two main seasons of the semi-arid Eastern Mediterranean climate
90 (short, mild and wet winter vs. long, hot and dry summer), offering a comprehensive understanding of the daily and monthly
91 variability of local and regional sources of carbonaceous aerosols. Cold and warm periods were compared to highlight the
92 complexity of local (combustion) sources and the importance of regional ones. These results were further processed to
93 apportion Black Carbon sources in Nicosia with emphasis on local versus regional contribution.

94 2. Material and Methods

95 2.1 Sampling site

96 **Cyprus:** Cyprus is the third largest island in the Mediterranean Sea, extending approximately 240km long from east-to-west
97 and 100km wide. The closest countries and their distance from the capital city of Nicosia are respectively Turkey (110km),
98 Syria (250km), Lebanon (250km), Israel (300km), Egypt (400km), Jordan (430 km), and Greece (900 km from the Greek
99 mainland), (Fig. 1a).

100 The population of Cyprus (~~approximately~~ 1 million inhabitants) is rather small compared to its neighbouring countries and
101 the rapidly growing (overall 400 million) population of the region (Lelieveld et al., 2013). The main urban areas of the island
102 shown in Fig. 1b, are those of Nicosia (c.a. 245,000 inhabitants), Limassol (c.a. 150,000 inhabitants), Larnaca (c.a. 50,000
103 inhabitants) and Paphos (c.a. 35,000 inhabitants). Cyprus has a Mediterranean and semi-arid climate with two main seasons:
104 a mild cold season (from December to March) and a hot warm season lasting about eight months (from April ~~to~~ November).
105 Rain occurs mainly in the cold season, with the warm one being extremely dry (i.e., almost no rain between May and
106 September)(Michaelides et al., 2018).

107 **Nicosia:** Nicosia is the largest city ~~on~~ the island and the southeasternmost of ~~the~~ European Union Member States' capitals.
108 Nicosia is currently partitioned in two, with a buffer zone in-between under the control of the United Nations; the southern
109 part being the capital of the Republic of Cyprus. The northern part of Nicosia (and ~~the~~ northern part of the island) is not
110 controlled by the government of the republic of Cyprus (Resolution 550, UN security council, 1984) (Fig. 1c). Geographically,
111 Nicosia is located in the centre of the island, within the Mesaoria plain, 150 m above sea level (asl), which is delimited on its
112 northern and southern edges by two mountain ranges; the Kyrenia Range culminating at 1,024 m asl, and the Troodos
113 Mountains culminating at 1,952 m asl, respectively. This topography channels winds within a more or less west-east corridor
114 (Fig. S5), feeding the city of Nicosia with long-range transported air masses from Europe, Africa, or the Middle East.

115 Measurements were performed at the Cyprus Atmospheric Observatory's Nicosia station (CAO-NIC) located at the Cyprus
116 Institute premises (Athalassa Campus; 174 m asl; 35.14N, 33.38E; Fig. 1c). The measurement site is considered ~~as~~ an urban
117 background site, located within a low population density residential area with no significant local pollution hotspots in its
118 vicinity (i.e., no dense road traffic, industry, commercial centers, restaurants, etc.) and next to the Athalassa Forestry Park.

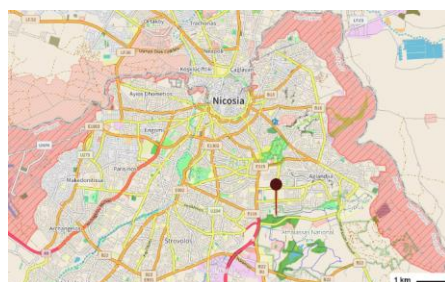
119 The period and duration of measurements presented here (07 December 2018 - 31 May 2019) were chosen to i) capture weather
120 conditions, atmospheric dynamics, and long-range pattern of the two main seasons, ii) investigate the contribution of domestic
121 heating emissions in winter, and iii) assess the potential increasing contribution of photochemical produced secondary aerosols
122 during the start of the dry and warm season. Local time (LT) in Cyprus is given as Eastern European Standard Time (EET)
123 (UTC+02:00 in winter and UTC+03:00 during the summer).



(a)



(b)



(c)

124 Figure 1: (a) Geographic location of the island of Cyprus and its closest Northern African and Middle Eastern neighbouring
 125 countries. (b) Location of the main cities of the Republic of Cyprus. Maps a,b were created by QGIS software v.3.26.3 utilizing the
 126 Natural Earth data (<https://qgis.org>). (c) Satellite view of the Nicosia agglomeration (grey area). The buffer zone dividing the island
 127 and the city is marked with red stripes; the location of the measurement site (CAO-NIC; The Cyprus Institute, Athalassa campus)
 128 is noted in red. (© OpenStreetMap contributors 2022. Distributed under the Open Data Commons Open Database License (ODbL)
 129 v1.0)

130 2.2 On-line Aerosol Instrumentation

131 On-line aerosol instrumentation has been operated following the Standard Operating Procedures defined by [ACTRIS](https://www.actris.eu)
 132 (<https://www.actris.eu>), the European Research Infrastructure on Aerosols, Clouds, and Trace Gases [ACTRIS](https://www.actris.eu)
 133 (<https://www.actris.eu>), and [Cost COLOSSAL \(CA16109, 2021\)](https://www.actris.eu).

134 Non-refractory submicron (NR-PM₁) aerosol chemical composition, i.e. organics, sulphate, nitrate, ammonium and chloride,
 135 was continuously monitored using a Quadrupole ACSM (Aerosol Chemical Speciation Monitor; Aerodyne Research Inc.) at
 136 a 30-min time resolution (Ng et al. 2011a). The instrument, along with a scanning mobility particle sizer (SMPS, described

137 below), sampled through a sharp cut cyclone operated at 4 L min⁻¹ (SCC 1.197, BGI Inc., USA), ~~and was equipped with a PM₁~~
 138 ~~aerodynamic lens, yielding an aerosol cut-off diameter of approximately 1.3µm. A nafion dryer was installed upstream,~~
 139 ~~keeping sample RH below 30%.~~ Data were retrieved using ACSM local v.1.6.0.3, implemented within Igor Pro (v. 6.37,

140 Wavemetrics Inc., USA). The ACSM is designed and built around similar technology as the aerosol mass spectrometer (Jayne
 141 et al., 2000), where an aerodynamic particle focusing lens is combined with particle flash vaporization in high vacuum ~~on the~~
 142 ~~surface of a standard tungsten vaporizer heated at 600 °C, followed by electron impact ionization, separation and final detection~~
 143 ~~of the resulting ions using a quadrupole mass spectrometer at 600 °C, electron impact ionization, separation and final detection~~
 144 ~~of the resulting ions using a quadrupole mass spectrometer.~~ Mass concentrations are ~~ealeulated-corrected for incomplete~~
 145 ~~detection due to particle bounce,~~ using ~~thea~~ chemical composition-dependent collection efficiency (CDCE) (Middlebrook et
 146 al., 2012). ~~The determined parameters, response factor (RF) and relative ionization efficiency (RIE) are reported in table S2.~~

147

Formatted: Default Paragraph Font

Formatted: English (United Kingdom)

148 Black carbon (BC) measurements were conducted using an ~~an~~ ~~AE-33~~ 7-wavelength aethalometer (~~AE-33~~ Magee Scientific, US)
149 at a 1-min time resolution. The aethalometer sampled ambient aerosol through a PM_{2.5} aerosol inlet (SCC 1.829, BGI Inc.,
150 USA) at a flow rate of 5 L min⁻¹; after passing through a nafion dryer. The instrument internally corrected the filter loading
151 effect in real-time, while a fixed value (C₀=1.39) was applied to compensate for the multi-scattering effect (Drinovec et al.,
152 2015). BC was apportioned to source specific components, namely BC_{ff} related to fossil fuel combustion and BC_{wb} related to
153 wood burning, by applying the "aethalometer model" (Sandradewi et al., 2008) on the 470 – 950 nm wavelength pair. ~~The~~
154 ~~using the~~ instrument's default values for fossil fuel combustion and wood-burning aerosol Absorption Ångström Exponent,
155 AAE_{ff}=1 and AAE_{wb}=2, respectively ~~were selected after performing a sensitivity analysis on the AAE values (Supplement~~
156 ~~Section 3).~~

157 2.3 Ancillary measurements

158 **SMPS:** Particle number size distributions were monitored using a scanning mobility particle sizer (SMPS) consisting of an
159 electrostatic classifier (model 3080, TSI Inc., USA) coupled with a condensation particle counter (CPC; model 3070, TSI Inc.
160 USA) operating at a 5-min time resolution and at a 1 L min⁻¹ sample flow rate, measuring particles with a diameter ranging
161 from 9 to 700 nm. Ambient aerosols were drawn through a nafion dryer, ~~and~~ placed upstream, keeping sample RH below 30
162 %. Volume concentrations of assumed spherical particles derived by the SMPS were converted into mass concentrations using
163 a variable density calculated by the methodology described in Bougiatioti et al. (2014). The respective mass fractions time
164 series of chemical species were calculated based on the ACSM measurements. A density value of 1.77 g cm⁻³ was used for
165 ammonium sulphate, and 1.35 g cm⁻³ for organics (Florou et al., 2017; Lee et al., 2010), the two dominant compounds of PM₁
166 in Nicosia as detailed further below.

167 **Filter sampling:** Co-located 24h PM_{2.5} samples were collected on quartz fiber filters (Tissuquartz, 47mm diameter, Pall) using
168 a low volume sampler (Leckel SEQ47/50) operating at a flowrate of 2.3 m³ h⁻¹. The filter samples were analysed for i) organic
169 and elemental carbon using an OC/EC Lab Instrument (Sunset Laboratory Inc., OR, USA) implementing the EUSAAR II
170 protocol (Cavalli and Putaud, 2008), ii) carbohydrates, including levoglucosan, mannosan, galactosan, using an Ion
171 Chromatography Pulsed Amperometric Detection method (Thermo - Model ICS-3000) and iii) anions (Cl⁻, NO₃⁻, SO₄²⁻, MSA,
172 Oxalate) and cations (K⁺, Na⁺, NH₄⁺, Mg²⁺, Ca²⁺) using ion chromatography (Thermo - Model ICS-5000).

173 **Proton Transfer Reaction - Mass Spectrometry (PTR-MS):** Air was sampled through a 20m long, 3/8" o.d. (1/4" i.d.)
174 sheathed Teflon line that ran from the roof of the building to the instrument. A Teflon filter (0.2µm diameter porosity) was
175 installed at the inlet to prevent large aerosol particles and insects from entering the sampling line. The resulting residence time
176 of air in the line was estimated to ~~be ea-~~ ~~approximately~~ 0.5 min. ~~The T-~~ temporal resolution of Volatile Organic Compounds
177 (VOCs) measured by the PTR-MS (Ionicon Analytik, Austria) was approximately two minutes (the time required to measure
178 55 different ions at 2 seconds per ion). The basic operation principles of the PTR-MS instrument have been described in detail
179 by Lindinger et al. (2011). Briefly, a stable flow of air and high concentrations of H₃O⁺ ions are continuously sampled into a
180 drift tube held at 2.2 mbar pressure. There, compounds with a proton affinity greater than water, including a large selection of
181 Oxygenated Volatile Organic Compounds (OVOCs), undergo efficient proton-transfer reactions with the H₃O⁺ ions to produce
182 protonated organic product ions, which can be detected by a mass spectrometer.

183 **Meteorological Parameters:** Standard meteorological parameters (temperature, relative humidity, wind speed and direction)
184 were obtained ~~174 asl0 m above ground at the Athalassa Forestry Park from the m~~ Meteorological station of the Cyprus
185 Department of Meteorology, ~~located installed 10 m above ground, located at the Athalassa Forestry Park (164 m asl) lying~~
186 ~~approximately at e.a.~~ 1.3 km east ~~from of the~~ CAO-NIC station. Wind speed and direction data were further used in this study
187 for component-specific non-parametric wind regression analysis (NWR) performed using the ZeFir toolbox (Petit et al., 2017)
188 developed within the Igor Pro software (Wavemetrics Inc.). A co-located automatic CIMEL CE370 micro-LIDAR was

189 operated continuously to retrieve the Planetary Boundary Layer Height (PBLH) and better assess the influence of atmospheric
190 dynamics on in-situ ground-based observations.

191 **Air masses back trajectory analysis:** Five-day air mass back trajectories arriving at 1000m altitude above the sampling site
192 were computed every 6 hours, using the Hybrid Single-Particle Lagrangian Integrated Trajectory model (HYPLIT4; Stein et
193 al., 2015) using the Global Data Assimilation System (GDAS 1) meteorological data fields (with 1° spatial resolution). Back
194 trajectories were coupled to measured concentrations, assessing origins and source contributions to specific chemical
195 components, by applying the Potential Source Contribution Function (PSCF) technique as implemented in the ZeFir toolbox
196 described above.

197 **2.4. Source Apportionment-Apportionment analysis**

198 Positive Matrix Factorization (PMF) is an advanced multivariate factor analysis tool that attempts to identify the contributing
199 factors, or sources, of atmospheric pollutants at a sampling site. For this study, source apportionment was performed on the
200 organic mass spectra dataset collected by the ACSM. The (PMF) method (Paatero and Tapper, 1994) using the multilinear
201 engine (ME-2) model developed by Paatero (1999) was implemented using the SoFi (Source Finder) toolkit (SoFi 6D;
202 Canonaco et al., 2013). PMF allows the decomposition of the OA mass spectra matrix X into two matrices, G and F and a
203 remaining residual matrix, E:

$$204 X = G * F + E \quad (1)$$

205 Where X is the input dataset matrix (measured quantity), F is the resulting source profile matrix, G is the source contribution
206 matrix (temporal variability of each source), and E represents the model residual matrix. Based on a number of criteria, the
207 optimal solution is selected, aiming at being physically meaningful that can be supported by external indicators (ancillary
208 measurements), and trying to minimize values in the residual matrix E. Model input data and error matrices (in $\mu\text{g m}^{-3}$), were
209 exported using the ACSM software. Data points with a signal-to-noise (S/N) ratio smaller than 0.2 were removed, and points
210 with S/N between 0.2 and 2 were down-weighted by increasing their estimated error values (Ulbrich et al., 2009; Paatero and
211 Hopke, 2003). m/z (mass-to-charge ratio) values ranging from 10 to 120 were used in the analysis. CO_2 -related variables
212 were excluded from the PMF and finally reinserted into the solution.

213 Source apportionment of OA was performed following the general steps described by Crippa et al. (2014) and the recently
214 updated harmonised standard operating procedures for seasonal OA PMF (Chen et al., 2022). As a first step, unconstrained
215 PMF analyses were performed with a number of factors ranging from 2 to 8 in order to identify the most relevant number of
216 factors and potential sources. If primary organic aerosol factor profiles such as Hydrocarbon-like OA (HOA), or biomass
217 burning-like OA (BBOA) were found, then the corresponding site-specific primary OA (POA) mass spectra (see discussion
218 below) or spectra found in the literature (e.g., Ng et al., (2011) and Crippa et al., (2014)) were set as constraints in the PMF,
219 using the “a-value” approach (Paatero and Hopke, 2009; Canonaco et al., 2013). A sensitivity analysis was then performed
220 with different a-values to assess the level of constrain introduced in each factor with: i) a constrained HOA using, as an anchor
221 the HOA spectrum found in Ng et al. (2011) with the a-values ranging between 0.05 and 2.0, ii) a constrained BBOA factor
222 with the a-values from 0.2 to 0.5 from Ng et al. (2011), and iii) a constrained cooking OA (COA) factor from Crippa et al.
223 (2014), Mohr et al. (2012) with a-values from 0.2 to 0.5. Once this sensitivity analysis was completed, the evaluation of the
224 PMF results showed that the BBOA factor could not account for the entire m/z 60 mass fragment, which fragment was
225 distributed within 2 factors. Additionally, the correlation of BBOA with BC_{wb} showed to be unsatisfactory (section S1). On
226 the other hand, given the BBOA factor’s sensitivity to the type of solid fuel used, different biomass-burning factor profiles
227 have been reported in various regions around the world (Mohr et al., 2012)(Xu et al., 2020; Trubetskaya et al., 2021)(Xu et
228 al., 2020; Trubetskaya et al., 2021)(Xu et al., 2020; Trubetskaya et al., 2021)(Xu et al., 2020; Trubetskaya et al., 2021)(Xu et
229 al., 2020; Trubetskaya et al., 2021)(Xu et al., 2020; Trubetskaya et al., 2021)(Xu et al., 2020; Trubetskaya et al., 2021).
230 Consequently, a site-specific BBOA factor profile (BBOA_{cy}) was selected. The BBOA_{cy} spectrum was calculated as an average
231 of 20 PMF runs from the initial unconstrained PMF for the cold period, validated by its time-series correlation to BC_{wb} . Since

232 aged OA (i.e. Oxygen-like OA, OOA) factors show more variability between measurement sites in terms of their mass spectra,
233 no constrain was introduced for these factors (Canonaco et al., 2015).

234 In this study, the BBOA factor - a major contributor of OA during winter - could not be properly resolved when performing
235 the PMF analysis on the entire period dataset. A seasonal approach was followed- instead, separating the OA dataset into two
236 periods that were then used to describe both the two periods (cold and warm, respectively). The criteria used to delineate those
237 two periods are presented and discussed in ~~the below~~ section 3.2.

238 One factor was consequentially constrained with the resulting BBOA_{cy} spectrum (with an a-value in the 0-0.5 range, using
239 steps of 0.02), obtaining the optimal solution using an a-value equal to 0.46. A widely referred-to standard mass spectrum (Sun
240 et al., 2016; Duan et al., 2020) derived from Ng et al. (2011) was used to constrain the HOA factor, with an a-value of 0.2,
241 thus obtaining the best correlation with BC_{fr}, a tracer for ~~traffie-traffic~~ related emissions. A detailed description of the OA
242 source apportionment analysis can be found in section S1 in the supplementary material.

243 3. Results and Discussion

244 3.1. On-line aerosol data quality check

245 A chemical mass closure exercise for PM₁ was performed at a temporal resolution of 1h to check the quality of the on-line
246 aerosol measurements. Chemically reconstructed PM₁ was calculated as the sum of the mass concentration of all non-refractory
247 species measured by the ACSM (OA, NO₃⁻, SO₄²⁻, NH₄⁺, Cl⁻) plus the BC concentrations measured by the Aethalometer AE-
248 33 (Putaud et al., 2004). The contribution of other chemical constituents to submicron aerosols, such as sea salt and dust
249 (measured by co-located filter sampling), was found to be low and therefore neglected here. A scatter plot of the ACSM + AE-
250 33 measurements vs. the SMPS-derived PM₁ concentrations is shown in Figure S4~~ab~~. The results ~~obtained~~ indicate a very
251 good correlation ($r^2 = 0.88$; N=1823) and a slope of 1.2 (Fig. S4~~ab~~). This 20% discrepancy lies within the uncertainty of the
252 on-line instruments ~~and~~. It could be attributed to the cut-off size of the SMPS at 700nm, ~~that which~~ is slightly lower compared
253 ~~to than~~ the ACSM. In addition, ACSM individual chemical species were compared with co-located off-line analyses performed
254 on daily PM_{2.5} filters. As shown in Fig. S4~~be-ef~~, very good agreement was obtained between on-line and off-line measurements
255 with $r^2 \geq 0.80$ (N=165-175) for all species. The discrepancy between ACSM and filter measurements for nitrate (slope of 1.3)
256 could ~~potentially~~ be attributed to the volatilization of HNO₃ from the filter surface due to the presence of semi-volatile
257 ammonium nitrate. The obtained slopes for ammonium and sulfate below 1:1 (0.81 and 0.85, respectively) ~~is-are~~ consistent
258 with the fact that fine (NH₄)₂SO₄ aerosols, mainly originating from secondary processes and long-range transport (Sciare et
259 al., 2010; Freutel et al., 2013), can be found at a large size mode possibly exceeding 1 μ m, consequently not being sampled by
260 the ACSM.

261 The study investigated the aerosol ion balance using both online and offline inorganic measurements. The ratio of the measured
262 concentration of NH₄⁺ Measured and the estimated concentration of NH₄⁺ Predicted, as calculated in (Jiang et al., (2019), was used for
263 this purpose. The results showed a slope of 0.80 for online measurements and 0.96 for offline measurements. These findings
264 suggest that the atmospheric aerosol observed during the study period was mostly fairly predominantly neutral, taking into
265 account the uncertainties of ammonium concentrations reported in Q-ACSM intercomparison studies (Crenn et al., 2015), as
266 well as the species' relatively high detection limit (Ng et al., 2011).

267 An very striking interesting result obtained from the comparison of OA (ACSM) with OC (from filters) is an OM-to-OC ratio
268 of 1.42 which is at the lower end of ratios reported for urban environments, which usually exhibit typical values of 1.6 ± 0.2
269 (Petit et al., 2015; Theodosi et al., 2011; Brown et al., 2013). Without neglecting the fact that two different size fractions were
270 compared (PM₁ for the ACSM and PM_{2.5} for the filter sampling), this low ratio probably point to long-chain hydrocarbon OA
271 that often are related to primary combustion (poorly oxidized) OA. This low ratio clearly denotes a major contribution of long-
272 chain hydrocarbon OA that often refer to primary combustion (poorly oxidized) OA (Aiken et al., 2008). As such, this ratio

273 could represent an independent means of verification of the consistency of our source apportionment between primary and
274 secondary OA.

275 ~~As such, this ratio will represent a valuable and independent means of verification of the consistency of our source~~
276 ~~apportionment between primary and secondary OA.~~

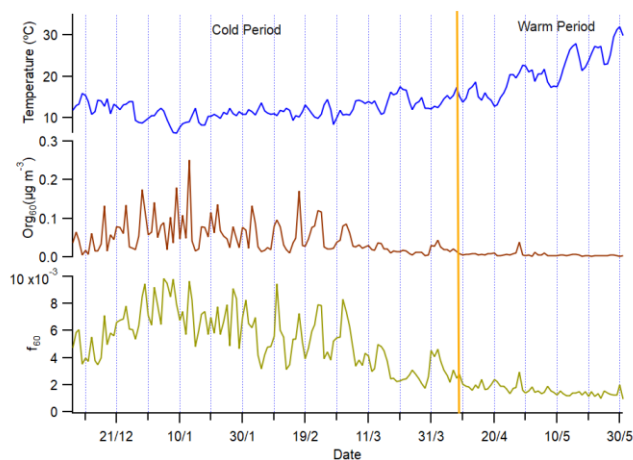
277 Finally, black carbon concentrations derived from light absorption measurements (Aethalometer AE-33) were compared
278 against filter-based EC measurements (see Fig. S4fa). Data from the two techniques correlate very well ($r^2=0.83$), with a
279 BC/EC ratio of 1.67 being similar to studies in other urban areas (Rigler et al., 2020; Liu et al., 2022), highlighting the existence
280 of a BC absorption enhancement (E_{abs}) attributable to a lensing effect induced by other chemical species, among which
281 secondary OA may play an important role (Zhang et al., 2018).

282

Formatted: English (United States)

283 3.2 Meteorological conditions

284 **Delineation of cold vs. warm seasons:** The ACSM organic mass at m/z (mass-to-charge-ratio)-60 is characteristic of the
285 fragmentation of levoglucosan, a product of cellulose pyrolysis and well-established biomass burning marker (Alfarra et al.,
286 2007). Its respective contribution to total OA (f_{60}) was used in this study as an indicator of biomass burning for domestic
287 heating to delineate cold vs. warm seasons, comparing with the 0.3% threshold proposed by Cubison et al., (2011) for air
288 masses influenced by biomass burning. Except for a single small peak in early May, corresponding to open fires for the
289 celebration of the Greek Orthodox Easter, the last instance when f_{60} was above the threshold was recorded during the first
290 week of April (Fig. 2). From then onwards, daily air temperature started rising constantly, from ~~about~~ 15°C ~~in~~ ~~at~~ the
291 beginning of April up to 30°C at the end of May. These two features dictated the division of the dataset into two periods: a
292 cold period of four months (07/12/2018-08/04/2019), with an average temperature of $12 \pm 4^\circ\text{C}$, and a warm period of two
293 months (09/04/2019 – 31/05/2019), with an average temperature of $20 \pm 7^\circ\text{C}$.



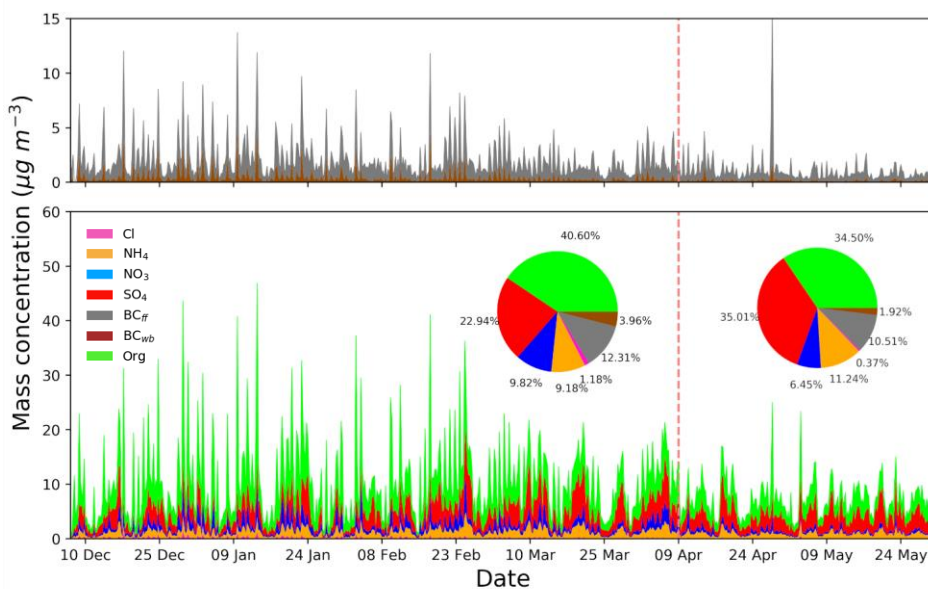
294
295 **Figure 2:** Time series of air temperature (blue), m/z 60 organic concentration (org60, brown) and f_{60} fragment (green) for the cold and warm
296 periods. The vertical line is used to delineate the measurements within the two seasons.

297 **Wind sectors:** During these two periods, a distinct pattern in the wind sectors and the air masses arriving at the sampling site
298 was observed. As seen in Fig. S5, the dominant wind direction for the cold period was the NW-SW [$225^\circ - 315^\circ$] sector
299 encompassing 48% of the total wind directions, while the NE-SE [$45^\circ - 135^\circ$] sector covered 26%. During the warm period,
300 the weight of this proportion is shifting even more towards the NW-SW [$225^\circ - 315^\circ$] sector, having a 62% of total air masses
301 while only 17% are arriving from the NE-SE [$45^\circ - 135^\circ$] sector.

302 **Air mass origin:** A cluster analysis was performed (Fig. S6a,b) for both periods in order to better assess the main upwind
 303 regions responsible for long-range transported air pollution over Cyprus and their change relative to the period of the year.
 304 The number of clusters used in each season was determined by considering the percentage change in Total Spatial Variance
 305 (TSV) as a function of the number of clusters of merged trajectories (Fig. S6c,d) and the mean trajectory paths of each cluster
 306 (Fig. S6e,f). The first large drops observed in TSV from the two – to – three and the three – to – four cluster transition could
 307 not represent all the recorded trajectories and especially the ones describing air masses arriving in Nicosia from the east. The
 308 next remarkable decrease in TSV was recorded when moving to seven clusters. Thus, for both periods, seven clusters were
 309 chosen to better represent all air masses arriving in Nicosia.
 310 A significant part of most of the calculated mean trajectory path representing clusters arriving in Cyprus was found to be
 311 related to the wider western sector, with many of them though, passing over Turkey before reaching Cyprus. Interestingly, this
 312 analysis showed one cluster (Cluster 1) arriving from the Middle East (close to Lebanon and Syria) and another four (Cluster
 313 1, 2, 5, 6) passing over the western part of Turkey for the cold period. For the warm period, the only clusters arriving from the
 314 Middle East were the ones related to Turkey (Clusters 1, 5, 6). Most of the air masses arriving in Cyprus were found to
 315 originate from Europe; many of them passing over Turkey before reaching Cyprus. Interestingly, this analysis showed one
 316 cluster arriving from Middle East for the cold period, whereas there were not enough trajectories passing
 317 Plotting all individual
 318 72h back trajectories (Fig S6e,f) showed that a clear portion (almost 25% of the calculated trajectories) are being influenced
 319 by the Middle East, especially for the cold period (Fig S6e). over the Middle East to calculate a cluster for this area during the
warm period.

3.3. Chemical composition of PM₁

321 **Seasonal perspective of PM₁:** The T_{ime} series of PM₁ chemical composition derived from the ACSM (OA, SO₄²⁻, NH₄⁺,
 322 NO₃⁻, Cl⁻) and the Aethalometer (BC_{fit}, BC_{wb}) are depicted for the entire measuring period in Figure 3. Averaged data (6h
 323 averaging period) are shown here for clarity. Furthermore, the relative average contribution of each chemical constituent to
 324 total PM₁ concentrations; is depicted in- the respective inserted-inner pie charts for both periods.



325

326 **Figure 3: Stacked area plots of the chemical composition** Time series of the chemical composition of PM₁ in Nicosia derived
 327 from 6-hour averages of ACSM and AE₃₃ measurements. The vertical dashed red line separates the cold from the warm season.
 328 The average relative contribution of each species is shown in the respective pie charts (inner panels) for each season.

329 Although intense and short-duration peaks are observed for carbonaceous aerosols (OA, BC_{ff}, BC_{wb}), background NR-PM₁
 330 concentration levels (between peak values) remain well below 10 µg m⁻³ for the 6-h average in both seasons. In other words,
 331 no PM₁ pollution episodes (with e.g., concentrations above 10 µg m⁻³) lasting for consecutive days were observed. Such lack
 332 of intense and persistent PM₁ pollution episodes differs from what is reported in central and northern Europe, where stagnant
 333 (anticyclonic) conditions occur together with continental (polluted) air masses, mainly in winter and springtime (e.g., Petit et
 334 al., 2015). This suggests that the relatively low emissions from Cyprus (compared to the neighboring countries) together
 335 with its remote marine location (i.e., far from densely populated areas) may prevent the build-up of high PM₁ pollution
 336 events over Nicosia. On the other hand, clear differences can be observed between both periods, with significantly higher PM₁
 337 concentrations during the cold period, associated with repeated, intense peaks of OA and BC - not observed during the warm
 338 season - and suggesting local combustion emissions. The highest PM₁ concentrations were observed between December 28th
 339 2018 and January 13th 2019 (Fig. 3) and were associated with low temperatures and Christmas holidays, both likely to promote
 340 the use of domestic heating. During the warm period, the higher contribution of sulfate, and lower
 341 contribution of OA, are clearly noticeable. The contribution of nitrate during the warm period, most probably in the form of
 342 semi-volatile NH₄NO₃, remains marginal, possibly due to non-favourable thermodynamic conditions preventing its formation
 343 and accumulation.

344 **PM₁ chemical composition:** For the cold period, the average calculated mass concentration of PM₁ (calculated as the sum of
 345 chemical components measured by AE₃₃ and ACSM) was 12.32-35 ± 9.77 µg m⁻³, with 10.340 ± 7.92 µg m⁻³ being the
 346 average concentration of the non-refractory species (Table 1). OA constitutes the larger fraction of PM₁ mass, with an average
 347 concentration of 5.03 ± 5.48 µg m⁻³ (41 %), followed by sulfate (23 %), black carbon (16 %), nitrate (10 %), ammonium (9
 348 %), and chloride (13 %). These concentrations and the overall distribution of chemical components in NR-PM₁ are quite similar
 349 to those measured by ACSM in other European cities (Bressi et al., 2021). Concentrations appear to decline during the warm
 350 period, with an average calculated PM₁ concentration of 8.18 ± 4.65 µg m⁻³, including 7.15-18 ± 3.80-81 µg m⁻³ from the non-
 351 refractory components. The dominant species during the warm period were sulfate and OA, each representing 35 % of PM₁,
 352 followed by black carbon (12 %), ammonium (11 %) and nitrate (6%). During that period, chloride concentrations were
 353 negligible, contributing less than 1 % (Table 1).

354 **Table 1: Species mean, standard deviation, median concentrations and respective contribution to PM₁ during cold and warm periods**
 355 **in Nicosia.**

| µg m ⁻³ | Cold Period | | | | Warm Period | | | |
|-------------------------------|-------------|------|--------|------------------|-------------|------|--------|------------------|
| | Mean | Std | Median | Contribution (%) | Mean | Std | Median | Contribution (%) |
| OA | 5.03 | 5.48 | 3.35 | 40.8141 | 2.83 | 1.91 | 2.51 | 34.5735 |
| SO ₄ ²⁻ | 2.844 | 1.89 | 2.60 | 22.8323 | 2.87 | 1.50 | 2.61 | 35.08 |
| NO ₃ ⁻ | 1.22 | 1.25 | 0.75 | 9.8710 | 0.53 | 0.56 | 0.34 | 6.46 |
| NH ₄ ⁺ | 1.14 | 0.77 | 1.01 | 9.259 | 0.92 | 0.55 | 0.84 | 11.30 |
| Cl ⁻ | 0.3114 | 1 | 0.2307 | 2.531 | 0.0503 | 8 | 0.012 | 0.62<1 |
| BC | 2.01 | 2.31 | 1.26 | 16.3316 | 1.01 | 1.46 | 0.66 | 12.36 |
| PM ₁ | 12.323 | 5 | 9.77 | 100.00 | 8.18 | 4.65 | 7.53 | 100.00 |

356
 357 Interestingly, sulfate concentrations recorded in Nicosia are much higher compared to what is commonly observed in other
 358 European countries and Mediterranean cities (Table 2) and likely reflect a regional pattern of sulfur-rich emissions compared
 359 to Europe, where SO₂ emissions have strongly decreased during the last decades (Smith et al., 2011; Chin et al., 2014) thanks

- Formatted: Font: Bold
- Formatted: Font: Bold, Not Superscript/ Subscript
- Formatted: Font: Bold
- Formatted: Font: Bold
- Formatted: Font: Bold, English (United Kingdom)
- Formatted: Font: Bold
- Formatted: English (United Kingdom), Check spelling and grammar

360 to the implementation of specific abatement measures on reducing sulfur emissions (European NEC Directive (EU, 2016) and
 361 United Nation Gothenburg (1999) protocol). More specifically, the importance of sulfur emissions in Turkey (2 455 Gg, EEA
 362 2021), which were 50% higher compared to the total SO_x emissions of the EU 28 in 2019, together with the fact that half of
 363 the air masses reaching Cyprus are passing over Turkey (see Fig. S6) are key contributors to the high concentrations of sulfate
 364 in our study.

365 Shipping emissions appear to have a relatively minor impact on the concentration of sulfate. To more accurately determine the
 366 contribution of shipping emissions to SO₄²⁻, SO₂, and total PM_{2.5} a supplementary analysis was conducted using the WRF-
 367 Chem model, which simulates both physical and chemical processes occurring in the atmosphere. This model has been
 368 extensively evaluated in several studies for the Eastern Mediterranean (Kushta et al., 2018) and Europe (Berger et al., 2016;
 369 Tuccella et al., 2012). Following the set-up used in (Giannakis et al., (2019) and driven by the EDGAR v.5 anthropogenic
 370 emission inventories (Crippa et al., 2019), two annual-long simulations were performed: firstly, including all sectoral emissions
 371 in the model (baseline simulation S₀) and a second simulation where shipping emissions have been omitted (scenario
 372 simulation, S₁) to identify the impact of shipping on gaseous and aerosol sulfur-related species concentrations (SO₂ and SO₄²⁻
 373) and total PM_{2.5} over the Central and Eastern Mediterranean. The figures (S final) describe the contribution of shipping in
 374 absolute terms (Fig. S7 a,c,e) and as a percentage (Fig. S7 b,d,f) for the SO₄²⁻, SO₂ and total PM_{2.5} calculated for each species.
 375 According to these results, the highest impact of shipping on near-ground modelled concentrations of the three species (SO₄²⁻
 376 , SO₂ and PM_{2.5}) was estimated along the central Mediterranean region (yellow grids, west of the Balkans and Greece), as
 377 well as a small section south of Greece. The Levantine basin, where Cyprus is located, experiences significantly lower
 378 influence under the no-shipping emissions sensitivity test. More specifically, over the East Mediterranean, SO₄²⁻ concentrations
 379 represent a relative change of only about 6-8% when including shipping emissions.

Formatted: Font: Not Italic

Formatted: Font: Not Italic

Formatted: English (United States)

381 **Table 2: Comparison of concentration, and percentage contribution to PM₁, between the main submicron chemical species derived**
 382 **by ACSM.**

| | PM ₁ (µg m ⁻³) | OA (µg m ⁻³) | SO ₄ ²⁻ (µg m ⁻³) | NH ₄ ⁺ (µg m ⁻³) | NO ₃ ⁻ (µg m ⁻³) | Cl ⁻ (µg m ⁻³) | Reference |
|--------------------------|--|-----------------------------|--|---|---|--|--------------------------|
| Nicosia Cold (DJFM) | 12.32 | 5.03 | 2.81 | 1.14 | 1.22 | 0.31 | This study |
| Nicosia Warm (AM) | 8.18 | 2.83 | 2.87 | 0.92 | 0.53 | 0.05 | This study |
| Cyprus RB* (Annual) | 7.6 | 3.26 | 2.66 | 0.98 | 0.23 | - | Chen et al. (2022) |
| European UB** (Annual) | 10.6 | 5.3 | 2.0 | - | 1.9 | - | Bressi et al. (2021) |
| S. Europe RB*** (Annual) | 6.3 | 3.5 | 1.3 | - | 0.8 | - | Bressi et al. (2021) |
| Athens Winter | 18.7 | 13.13 | 2.4 | - | 1.8 | 0.14 | Stavroulas et al. (2019) |
| Athens Spring | 6.42 | 3.3 | 2.1 | 0.6 | 0.4 | 0.02 | Stavroulas et al. (2019) |
| Marseille Winter | 11.9 | 6.17 | 1.12 | 0.86 | 1.58 | 0.09 | Chazeau et al. (2021) |
| Marseille Spring | 8.09 | 3.86 | 1.06 | 0.70 | 1.13 | 0.04 | Chazeau et al. (2021) |
| Barcelona (Annual) | 9.85 | 4.10 | 1.70 | 1.05 | 1.35 | 0.06 | Via et al. (2021) |

Formatted: Font: 8 pt

383 * Cyprus Regional background

384 ** European urban background = Barcelona (Spain) + London (UK) + Prague (Czech) + Tartu (Estonia) + Zurich (Switzerland)

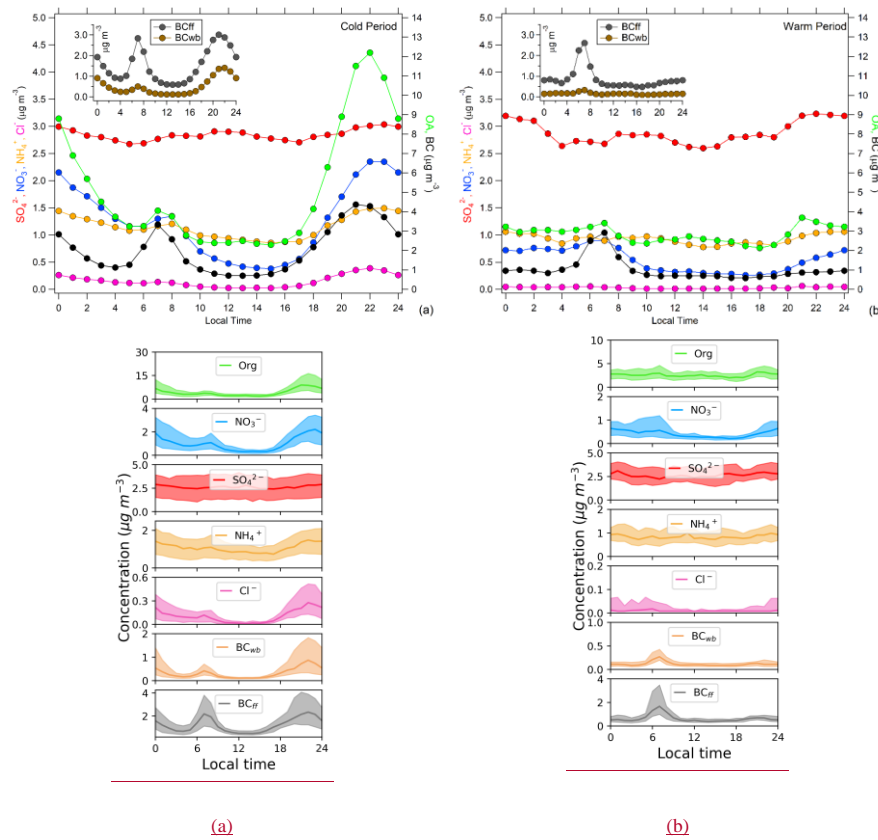
385 ***Southern European regional background = Ersu (Corsica, France) + Finokalia (Crete, Greece)

386 The main difference between the cold and warm periods lies in the decrease of in the concentration of carbonaceous aerosols
 387 (OA, BC) and NO₃⁻ by almost a factor of two. Several phenomena can explain this significant seasonal variation: the absence
 388 of a domestic heating source (mainly biomass burning as explained in Fig. 2); the absence of Middle East air masses during
 389 the warm period (see discussion later on); the increase in the Planetary Boundary Layer Height (PBLH) above Nicosia (Fig.
 390 S87) enhancing vertical dilution of local emissions during the warm period and therefore lowering ground-based
 391 concentrations; less favourable thermodynamic conditions, with warmer and dryer air, also preventing the condensation of

392 semi-volatile species (e.g., ammonium nitrate). Sulfate concentrations do not exhibit a similar seasonal pattern and therefore
 393 seem to be less affected by the above factors. On the contrary, the increase in photochemistry enhances the formation of sulfate
 394 aerosols, and the decrease in precipitation enhances aerosol lifetime, ~~strengthening~~ strengthening the impact of long-range
 395 transport.

396 3.4. Diurnal variability of PM₁ chemical constituents

397 Figure 4 shows the diurnal variability of the PM₁ species derived from the ACSM and AE-33 for both the cold (Fig. 4a) and
 398 warm (Fig. 4b) periods. The diurnal variability of the apportioned BC related to fossil fuel combustion (BC_{ff}) and wood-
 399 burning (BC_{wb}) are also depicted here.



Formatted Table

400 **Figure 4:** Median diurnal variability trends of the main submicron chemical constituents (OA, SO₄²⁻, NO₃⁻, NH₄⁺, Cl⁻ and BC) during the
 401 a) cold and b) warm periods. The diurnal profiles of BC_{ff} and BC_{wb} are embedded. Shaded area represents the 25th and 75th percentiles of
 402 the diurnals.

Formatted: Superscript

Formatted: Superscript

403 **Organic aerosols:** Organic aerosols ~~clearly~~ clearly dominate the cold period PM₁ concentration levels, exhibiting a night-time
 404 maximum above 12 µg m⁻³; and a second smaller maximum at 4 µg m⁻³, coinciding with local traffic rush hour (06:00-09:00
 405 LT). Elevated OA concentrations in the cold period during the night (max at 22:00 LT) are a common, well-documented
 406 feature in many urban environments across Europe and the Mediterranean (e.g., Florou et al., 2017; Stavroulas et al., 2019;
 407 Chazeau et al., 2021). They can be attributed to higher emissions from domestic heating, evening traffic peak and cooking

408 activities. The strong correlation between OA and BC_{wb} ($R^2=0.81$; $N=2934$; Fig. S98) suggests that residential wood burning
409 is an important contributor to this nighttime peak. Interestingly, this peak is not significantly amplified by a lower PBLH
410 during night-time, which seems to remain relatively stable with no significant diurnal variability during the cold period (Fig.
411 S87). It is also worth noting that background OA concentrations observed both at the end of the night and middle of the day,
412 when local emissions are minimal, remain relatively high at aroundea: $3 \mu\text{g m}^{-3}$. The diurnal variability of OA is much less
413 pronounced during the warm period, suggesting a more important contribution of regional sources to OA compared to the
414 strong dynamic of local emissions. The assumption of a more important contribution from regional OA during the warm period
415 is further supported by a mean OA concentration of $2.83 \mu\text{g m}^{-3}$ (Table 2) that is close to the averaged OA concentrations of
416 $3.2 \mu\text{g m}^{-3}$ reported for a 2-year period continuous observations with Q-ACSM (2015-2016) at the rural background site of the
417 Cyprus Atmospheric Observatory at Agia Marian Xyliatou (CAO-AMX), at aea-40km distance roughly 40 km from Nicosia
418 (Chen et al., 2022). During the warm period, a small OA peak remains visible in the morning, with a similar amplitude to
419 the cold season, likely to be related to traffic emissions. A second peak can be observed at 21:00 LT (not observed in BC),
420 which may possibly originatepotentially originating from cooking activities. Heavy oil combustion from shipping could
421 possibly contribute to OA. Further to the poor contribution of shipping emission on OA, a model study of sources of organic
422 aerosols in Europe using CAMx (Jiang et al., 2019) showed that the contribution of "other anthropogenic sources" (gathering
423 shipping, industry, and energy production) on OA (POA+SOA) was, typically, of the order of 10% during summer and winter
424 in the Eastern Mediterranean region close to Cyprus. Based on a simple receptor model, PM_{2.5} source apportionment performed
425 in Nicosia, Achilleos et al. (2016) showed that the contribution from shipping is approximately 8% to PM_{2.5}. Most of the
426 transported mass is attributed to SO₄²⁻ with a minor contribution from carbonaceous aerosols. In conclusion, shipping emissions
427 are likely to play a minor role in OA concentrations.

428 **Black carbon:** During the cold season, BC follows a bimodal diurnal pattern, which can be further apportioned by focusing
429 on its source-specific components BC_{fr} and BC_{wb}. The fossil fuel component exhibits two maxima, one in the early morning,
430 coinciding with traffic rush hour, and one in the late afternoon, most probably related to both traffic and an increase in energy
431 demand due to domestic heating (see discussion later on). On the other hand, BC_{wb} diurnal variability is dominated by a night-
432 time maximum (20:00 - 01:00 LT), peaking one hour after BC_{fr} and linked to wintertime residential wood-burning emissions,
433 contributing up to 33 % of total BC. During the warm season, the BC diurnal pattern is characterised by the absence of a night-
434 time maximum, while still exhibiting a significant peak in the morning, dominated by BC_{fr}. The very low contribution of
435 biomass-related combustion particles during the warm period, as previously noted from m/z 60 in Fig. 2, is further supported
436 here, with BC_{wb} exhibiting a nearly flat diurnal variability with close-to-zero mass concentrations. The contribution of shipping
437 in the Mediterranean on Black Carbon (BC) concentrations was investigated from model estimates by (Marmer et al., (2009)
438 based on three (3) most commonly used ship emissions inventories: 1) EDGAR FT by (Olivier et al., (2005), 2) (Eyring et al.,
439 (2005), and 3) EMEP by Vestreng et al. (2007). Results showed that shipping emissions were contributing to typically 15-25%
440 of BC in the E. Mediterranean, far from the shipping routes (which is the case for Cyprus). A similar result was found from a
441 more detailed (Positive Matrix Factorization) PM_{2.5} source apportionment analysis performed in Nicosia in 2018, with heavy
442 oil combustion contributing 7% to PM_{2.5} (Bimenyimana et al., 2023 under review), and the relevant factor containing less than
443 0.1 $\mu\text{g m}^{-3}$ of EC.

444 **Secondary inorganic aerosols:** During the cold season, non-refractory nitrate and chloride detected by the Q-ACSM are
445 mostly present in the form of semi-volatile NH_4NO_3 and NH_4Cl (Guo et al., 2017; Theodosi et al., 2018). They show a night-
446 time maximum (Fig. 4-a), reflecting the presence of gas precursors (NH_3 , HNO_3 , HCl) and the more favourable thermodynamic
447 conditions with lower temperatures, higher relative humidity, and condensation sink due to high PM concentrations of
448 combustion aerosols (traffic, domestic heating). Additionally, there is a smaller morning NO_3^- peak, most probably linked to
449 traffic (Foret et al., 2022). This is not observed for chloride, suggesting that HCl may not be as abundant in the morning

Formatted: Subscript

Formatted: Subscript

Formatted: Subscript

Formatted: Subscript

450 compared to the evening. The less favourable thermodynamic conditions during the warm period leads to very small
451 concentrations of semi-volatile NO_3^- and Cl^- (Fig. 4b). As expected, sulfate does not show a pronounced diurnal pattern,
452 irrespective of the period, and pointing to regionally-processed aerosols (Fig. 4a,b).

453 3.5. OA Source Apportionment

454 3.5.1 OA source apportionment during the cold period

455 For the cold period, the optimal PMF result has been found using a 5-factor solution following the approach detailed in section
456 2.4. The identification of OA sources related to these 5 factors was then performed following the typical combination of
457 information from i) OA mass spectra (Fig. S9a), ii) the correlation of each factor with source-specific tracers (see Fig. 5b),
458 iii) their diurnal variability (Fig. 6a), and iv) their daily (week days vs. week-end) pattern (also Fig. 6b). The five factors were
459 then assigned to the following sources: A primary BBOA (Biomass Burning Organic Aerosol), two primary HOA
460 (Hydrocarbon-like Organic Aerosol; HOA-1 and HOA-2) and two secondary OA sources, namely low-volatile MO-OOA
461 (Low-volatile-More-Oxidized Oxygenated Organic Aerosol) and semi-volatile LO-OOA (Semi-volatile-Less-Oxidized
462 Oxygenated Organic Aerosol). This source apportionment is presented and justified below for each factor:

463 **HOA-1 (Hydrocarbon-Like OA Type 1):** The mass spectrum of HOA-1 (Fig. S9a5a) is consistent with a fossil fuel (traffic)
464 combustion source that can be identified by the prevailing contributions of the ion series representing $\text{C}_n\text{H}_{2n-1}$ ($m/z = 27, 41,$
465 $55, 69, 83, 97$, typical fragments of cycloalkanes or unsaturated hydrocarbon chains) and $\text{C}_n\text{H}_{2n+1}$ ($m/z = 29, 43, 57, 71, 85,$
466 99 , typical fragments of alkane chains). Hence, this factor mass spectrum is well correlated to eight selected HOA factors
467 related to vehicular traffic found in the literature (Fig. S10a) and relevant to European and Mediterranean environments. The
468 traffic-related origin of the HOA-1 factor can be further confirmed by the good correlation with BC_{fr} ($R^2=0.65$; $N=2934$; Fig.
469 S11a), benzene ($R^2=0.72$; $N=1165$; Fig. S11b). The diurnal variability of HOA-1 shows a bimodal cycle with a sharp maximum
470 during the morning rush hour with an amplitude similar to BC_{fr} (Fig. 6a), and a broader maximum in the evening possibly
471 encompassing emissions from traffic and diesel-fired residential heating systems. In the weekly cycle, as depicted in Fig. 6b,
472 the morning peak decreases ~~in-on~~ Saturday ~~and~~. It is nearly absent on Sunday mornings, aligned with the de-escalation of
473 traffic emissions usually observed during weekend mornings.

474
475 **BBOA (Biomass Burning OA):** The mass spectrum of the site-specific BBOA factor (reported as BBOA_{cy} in section 2.4)
476 exhibits characteristic peaks at m/z 29, 60, and 73 (Fig. S9a5a), which are indicative of biomass burning (Crippa et al., 2014).
477 The mass spectrum is quite similar to other BBOA spectra found in the Mediterranean and Europe (Fig. S10c), with a key
478 difference here being the rather low contribution of a signal at $m/z=43$. The biomass burning-related origin of the factor is
479 further confirmed by the strong correlation with BC_{wb} ($R^2=0.81$; $N=2934$; Fig. S11c), benzene ($R^2=0.61$; $N=1162$; Fig. S11d)
480 and levoglucosan ($R^2=0.94$; $N=125$; Fig. S11e) a typical tracer of biomass burning (Fourtziou et al., 2017). The BBOA diurnal
481 pattern exhibits an expected well-marked night-time maximum around 22:00 LT, consistent with residential wood-burning
482 activities. This night-time maximum is observed throughout the week (Fig. 6a), confirming the important role of wood burning
483 for heating in the city. Interestingly, the higher concentrations of BBOA as well as BC_{wb} (Fig. 6b) were observed on Sunday
484 evenings, pointing to athe recreational use of fireplaces, leading to enhanced residential wood-burning emissions during the
485 weekend, a feature also reported in other sites in Europe and the US (Bressi et al., 2016; Rattanavaraha et al., 2017; Zhang et
486 al., 2019).

487 **HOA-2 (Hydrocarbon-Like OA Type 2):** The mass spectrum obtained for this factor (Fig. S9a5a) is similar to the HOA-1
488 factor, with high signals for the ion series $\text{C}_n\text{H}_{2n+1}^+$ and $\text{C}_n\text{H}_{2n-1}^+$. The main differences between these two factors occur in the
489 relative contribution of m/z 41 compared to m/z 43 and the relative contribution of m/z 55 compared to m/z 57, which are both
490 much higher for HOA-2, than for HOA-1. Furthermore, the contribution of signal to m/z 44 is more significant in HOA-2,
491 which can imply a mix of various sources and/or a possible possibly higher degree of atmospheric processing. Other

492 discrepancies with HOA-1 concern its diurnal variability, with an intense maximum at night (Fig. 6a), and ~~even more~~ its
493 average concentration levels, which are almost three times higher than HOA-1.

494 **Influence of cooking activities:** The HOA-2 diurnal profile has a small peak at 13:00 LT and a significantly higher one at 21:00
495 LT, effectively coinciding with typical meal times in Cyprus as well as those reported in the literature for Greece (Siouti et al.,
496 2021), therefore indicating the influence of cooking activities to this factor. When plotting f_{55} vs f_{57} (Mohr et al., 2012) and
497 colouring the data points by the corresponding time of day, a distinct pattern appears with data of higher f_{55} over f_{57} being
498 clustered to the top left of the triangle, close to the fitted lines representing cooking (Fig. S12) and coinciding with midday and
499 evening hours. The night-time maxima pattern is consistent throughout the week, with the higher concentrations being recorded
500 on Friday and Saturday evenings (Fig. 6b), in line with an expected food service sector activity increase as part of Nicosia
501 inhabitants' leisure in the weekend. The mass spectrum of HOA-2, even though left unconstrained, is highly correlated to COA
502 found in other studies (Fig. S10b) in both Mediterranean and continental European urban environments. Additionally, the non-
503 negligible signal at $m/z=60$ points to the widely spread habit of meat charbroiling (Kaltsonoudis et al., 2017).

504 **Influence of power plant emissions:** A closer look at the diurnal variability of the HOA-2 factor shows a certain persistence of
505 this factor throughout the day, even when cooking activities are more or less absent (Fig. 6a). Such pattern could imply the
506 influence of other combustion sources, not necessarily of local origin. The influence of other combustion sources would also
507 help to explain why HOA-2 average concentrations are roughly 3 times higher than OA related to traffic (HOA-1), as it is very
508 unlikely that cooking activities can contribute solely to the observed HOA-2 concentrations. A possible contributing source
509 could be related to the energy production sector ~~in-on~~ the island, which relies exclusively on heavy fuel oil. In a recent study,
510 Vrekoussis et al. (2022), utilizing satellite observations, have identified that power plants located to the North (Tekneik
511 powerplant, PP4, 362MW), North-East (Kalecik powerplant, PP5, 153MW) and South-East (Dhekelia power station, PP3,
512 460MW) of Nicosia at 22 km, 60 km and 38 km, respectively, are significantly contributing to columnar NO_2 concentrations
513 over the island. The importance of these emission hotspots, along with their location on the island, during both the cold and
514 warm periods is illustrated in Fig. S13 and shows, ~~in-particular~~ particularly for the Northern power plants (PP4, PP5), emissions
515 as high as the traffic-related NO_2 over Nicosia. Interestingly, in a source apportioning study on VOCs performed at the Cyprus
516 Atmospheric Observatory – Agia Marina Xyliatou (CAO-AMX), a rural remote site 32 km southwest of Nicosia, Debevec et
517 al. (2017) have resolved a factor related to industrial activity/power generation, exhibiting a connection with winds arriving
518 from the wider eastern sector.

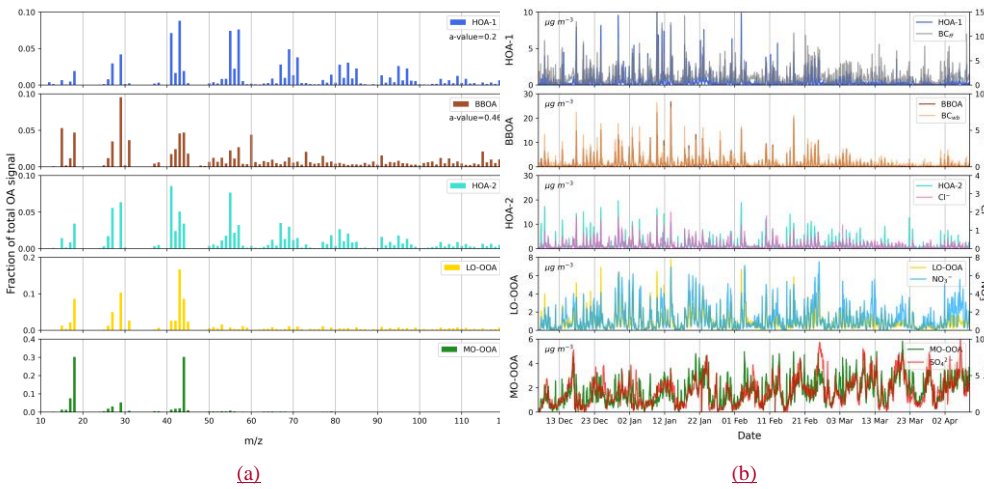
519 In order to assess the possible influence of Cypriot power plant emissions, the coupling of wind velocity, ~~and~~ wind direction
520 with the HOA-2 time-series was performed through NWR analysis (Fig S14b). This analysis highlights the association of
521 stagnant conditions (low wind speed / low dispersion) with high HOA-2 concentrations (i.e., night-time peaks), pointing to a
522 more local origin for this OA source. On the other hand, different features appear when wind velocities are higher, showing
523 emissions originating from the NW and the E-NE sectors; i.e. downwind of power plants PP4; and PP5, although long-range
524 transport influence cannot be ruled out. This is illustrated by the NWR of sulfate (Fig. S14f), which shows a dominant E sector
525 likely to originate from regional emissions. Given the positioning of the sampling site, close to the edge of ~~Nicosia's~~ Nicosia
526 urban fabric, with the Athalassa park lying to the east, such an observation can suggest the transport of plumes from the
527 operating powerplants, namely PP5 and PP3 to the city. Interestingly, a similar, yet even clearer image stands for SO_2
528 concentrations – only half – of which are considered to be of urban origin (Vrekoussis et al., 2022) – measured at a suburban
529 background site (NicRes) and a traffic site (NicTra) in the city (Fig. S14g-h), with elevated SO_2 concentrations being related
530 to eastern winds of higher velocity, further corroborating that power generation related polluted plumes, traveling through the
531 Mesaoria plain arriving to Nicosia can contribute to the HOA-2 factor.

532 Other combustion sources: Interestingly, chloride shows a good correlation with HOA-2 ($r^2=0.61$; $N=2945$; see Fig. S11f, Fig.
533 5b). Chloride detected by the ACSM is in the form of NH_4Cl (a secondary highly-volatile species). The source of this chloride
534 is still widely debated and may originate from industrial activity or municipal (plastic-containing) waste burning (Gunthe et

535 al., 2021). Another possible explanation of the good agreement between HOA-2 and chloride would be the use of Cl-rich coal
536 as a means for outdoor cooking in Nicosia could therefore reflect the influence of cooking activities that comprises a fraction
537 of the HOA-2 factor.

538 **Less-Oxidized Oxygenated OA (LO-OOA):** With elevated contribution of m/z 44, the mass spectrum of this factor is
539 consistent with a secondary OOA source. A higher m/z 43; and a lower m/z 44 (Fig. S9a5a) compared to MO-OOA; implies a
540 less oxygenated (less-processed) component (Mohr et al., 2012). Finally, the time series of this factor is quite similar to NO₃,
541 with an overall good correlation value ($R^2 = 0.67$, N=2943; Fig. S11h), highlighting its semi-volatile character. This is further
542 corroborated by the very good correlation of LO-OOA with chloride ($R^2 = 0.73$, N=2943; Fig S11i), another semi-volatile
543 compound measured by the Q-ACSM. The diurnal variation of LO-OOA displays 1.5 times higher concentrations during the
544 night compared to daytime (maximum of $1.84 \pm 0.31 \mu\text{g m}^{-3}$ at 22:00 LT; Fig. 6a); a pattern that is much more pronounced
545 than the variability observed for MO-OOA. This feature highlights ~~the fact~~ that the presence of LO-OOA, is not exclusively
546 controlled by photochemical processes. Instead, changes in thermodynamic equilibrium (due to lower T and increased RH),
547 favouring the condensation of gas-phase semi-volatile material on ~~the~~ one hand, and intense night-time chemistry (gas phase
548 or heterogenous) on the other hand, are among the processes that may account for the rapid night-time formation of LO-OOA.
549 Atmospheric processing of biomass burning OA during periods of low photochemical activity (such as in winter or at night),
550 ~~known also known~~ as “dark” aging, ~~have-has~~ been reported recently (Kodros et al., 2020; Jorga et al., 2021) and could
551 have contributed to the observed night-time formation of LO-OOA. Notably, the weekly cycle of LO-OOA, and its night-time
552 maxima, appears to have the same pattern and intensity as those observed for BBOA (e.g., low peaks on Tuesday/Thursday,
553 maximum on Sunday) (Fig. 6b). On the other hand, the factor is correlated with both BBOA ($R^2=0.81$; Fig. S11k) and BC_{wb}
554 ($R^2=0.66$; Fig. S11j). This observation could indicate a biomass-burning contribution to LO-OOA; through fast oxidation of
555 primary emissions, supported ~~in-by~~ several studies showing biomass burning linked ~~to~~ OOA sources at night (Stavroulas et
556 al., 2019; Kodros et al., 2020; Chen et al., 2021).

557 **More-Oxidized Oxygenated OA (MO-OOA):** The MO-OOA factor typically accounts for secondary organic aerosol formed
558 in the atmosphere from gas-to-particle conversion processes of VOCs and their products, as well as atmospheric ageing of
559 primary OA (Petit et al., 2015; Stavroulas et al., 2019). Numerous VOC sources can contribute to OOA but lose their mass
560 spectrum fingerprint owing to extended oxidation due to photochemical aging, which leads to enhanced signal at the m/z 44
561 fragment (CO₂⁺), a dominant tracer for OOA (Ng et al., 2011). The predominance of m/z 44 and the near absence of m/z 43 in
562 the mass spectrum of the resolved MO-OOA factor (Fig. S9a5a) points to highly oxidized/aged secondary OA (i.e., originating
563 from long-range transport). This is further supported by the relatively good agreement ($R^2=0.55$; N=2943; Fig. S11l) between
564 concentrations of MO-OOA and sulfate (Fig. 5b), a species of regional origin (Sciare et al., 2003). Nevertheless, the diurnal
565 variability of MO-OOA does not closely follow sulfate showing a small increase of 20-30% every evening (Fig. 6a,b), which
566 furthermore cannot be explained by atmospheric dynamics (c.f. the negligible PBLH diurnal variability for the cold period
567 shown in Fig. S87). Alternatively, this would suggest that a fraction of MO-OOA is produced locally through night-time
568 oxidation mechanisms as previously observed for LO-OOA. Similar nighttime increases of high oxygenated OA factors,
569 related to local sources, have been reported in both northern European urban sites (Zhang et al., 2019; Lin et al., 2022) as well
570 as in the Eastern Mediterranean urban environment (Athens, Greece), where a link to oxidized primary residential wood
571 burning emissions as a potential driver of the low volatility OOA factor diurnal variability, was also suggested (Stavroulas et
572 al., 2019).

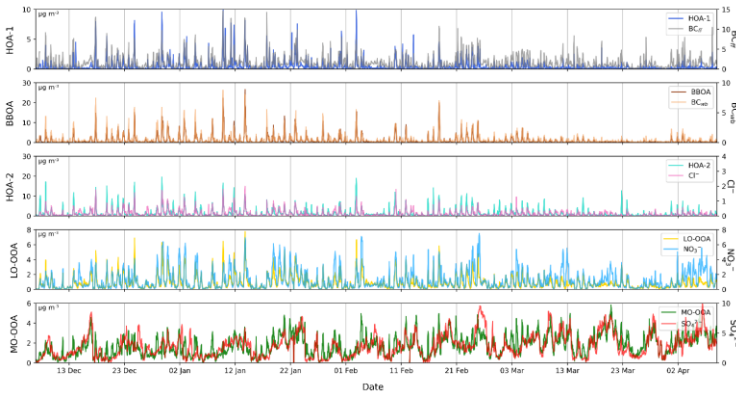


(a)

(b)

Formatted: Centered

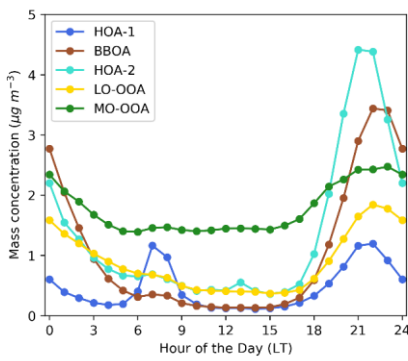
573



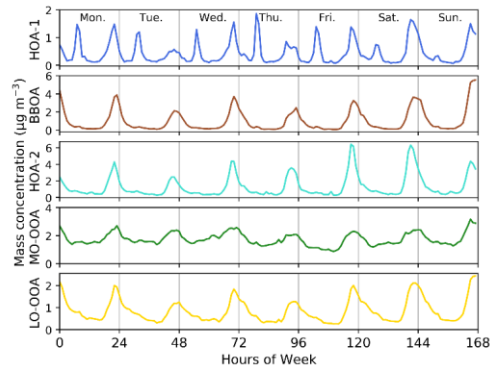
574

575 **Figure 5: Mass spectra of the PMF (a) and Time series of the five OA factors resolved along with corresponding tracer compounds**
 576 **(b) for the cold period.**

Formatted: English (United States)



(a)



(b)

577 **Figure 6: Diurnal variability (left) and weekly cycles (right) of the five OA factors averaged over the cold period..**

578 3.5.2. OA source apportionment during the warm period

579 For the warm period, the optimal PMF solution was obtained using a 4-factor solution (HOA-1, HOA-2, MO-OOA, LO-OOA).
580 As expected, the BBOA factor could not be resolved, as previously highlighted by the low concentrations at m/z 60 reported
581 during this period (Fig.2). Again, the identification of OA sources related to the 4 OA factors was performed following the
582 typical combination of information from i) OA mass spectra (Fig. S9b7a), ii) the correlation of each factor with external source-
583 specific tracers (Fig. 7b and Fig. S15), iii) their diurnal variability (Fig. 8a), and iv) their daily (week-days vs. week-end)
584 pattern (also Fig. 8b). The mass spectra profiles for the 4-factor PMF solution during the warm period (Fig. S9b7a) were quite
585 similar to the ones from the cold period (Fig. S9a5a).

586 **HOA-1:** For the warm period, an α -value of 0.2 was selected for constraining the HOA-1 factor, again using the Ng et al.
587 (2011b) HOA profile as a reference. The resolved factor profile is nearly identical to the one obtained for the cold season (R^2
588 = 0.99, Fig. S10a). and It is also very well correlated to traffic-related HOA factor profiles found in other Mediterranean
589 (Kostenedou et al., 2015; Gilardoni et al., 2016; Florou et al., 2017; Stavroulas et al., 2019) and European cities (Lanz et al.,
590 2010; Crippa et al., 2014) as depicted in detail in Fig S10a. The HOA-1 time series follows the same pattern as the
591 corresponding traffic-related HOA-1 factor reported for the cold period, showing a good correlation with BC_{fit} ($R^2=0.62$,
592 $N=1259$; Fig. S15a). Its diurnal variability exhibits a bimodal pattern, with a typical sharp maximum in the morning (07:00
593 LT) and a smaller peak during the evening (Fig. 8a). On a weekly basis, this diurnal variability tends to be less pronounced on
594 Saturdays and nearly absent on Sundays (Fig. 8b), reflecting reduced commuting during the weekend.

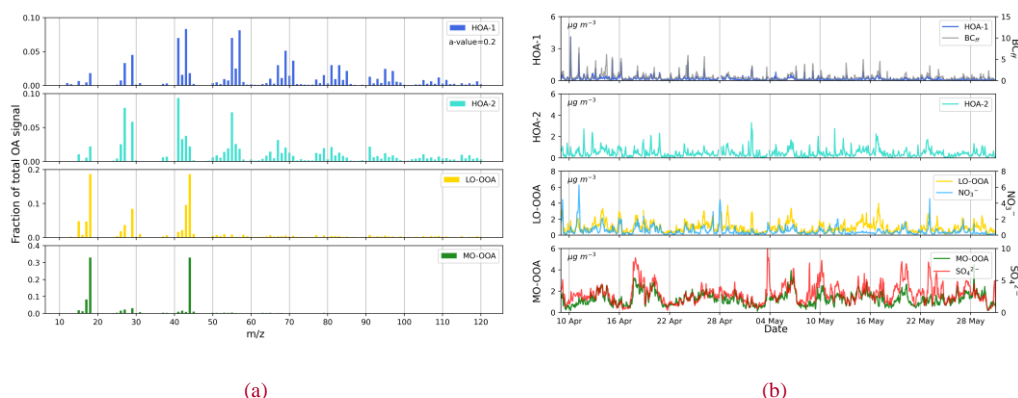
595 **HOA-2:** The HOA-2 factor still shows elevated concentrations during the warm period, close to 3 times higher compared
596 to HOA-1 (Table S32). The profile remains quite unchanged between the cold and warm periods ($R^2=0.92$; Fig. S10b),
597 pointing to similar sources. No correlation was observed with chloride, which may be expected due to unfavourable
598 thermodynamic conditions hindering NH_4Cl formation as well as the lack of significant chloride sources during this period. A
599 night-time maximum of HOA-2 is still observed when investigating the factor's diurnal variability (Fig. 8a). Furthermore, a
600 somewhat broader, compared to the cold period, maximum in the middle of the day (Fig. 8a) can also be observed. When
601 going through the weekly variability, this midday maximum is particularly well defined on Sundays (Fig. 8b), while the
602 evening peaks of Sundays and Mondays are the lowest. The above observations remain consistent with the cold period
603 assessment, that HOA-2 is on the one hand linked to cooking activities. For households activities are expected at noon and
604 evenings, while for restaurants, activity peaks on Sunday noon and is lower on Sunday evening and Monday, reflecting the
605 fact that such businesses remain closed on the first day of the week (Fig. 8b). On the other hand, the overall offset of HOA-2
606 observed against the HOA-1 diurnal profile persists, suggesting somewhat permanent background HOA-2 concentrations that
607 cannot be explained by cooking activities alone. A contribution to this source by continuous emissions from power plants (see
608 space-based (SP5-TROPOMI) vertical columns of NO_2 during the warm period in Fig.S13d); should be sought. In addition,
609 the HOA-2 NWR plot for the warm period reveals an even more significant enhancement of concentrations when moderate
610 winds blow from the E-SE (Fig. S16b), a trend also observed for SO_2 during the same period (Fig S16e,f).

611 The above observations remain consistent with our assessment for the cold period: the HOA-2 factor consists of a mixed OA
612 source that contains cooking activities (inc. coal combustion) and emissions from the powerplants located on the eastern part
613 of the island. Indeed, the HOA-2 midday maximum can be linked to an increase in electricity demand at that time of day during
614 the warm period due to an increase in air conditioning usage (Cyprus' NECP 2021-2030, 2019).

615 **LO-OOA:** The LO-OOA factor profile exhibits some differences with from the one resolved for the cold period ($R^2 = 0.66$),
616 as illustrated in the correlation matrix of comparison to selected factor profiles found in the literature (Fig. S10d) while being
617 very similar to those obtained in Athens/Piraeus during summer (Bougiatioti et al., 2014; Stavroulas et al., 2021). The LO-
618 OOA time-series shows a low agreement with NO_3^- ($R^2 = 0.31$; $N=1259$; Fig. S15c) poorer than the observed correlation
619 during the cold period (Fig. S11h). The diurnal pattern of the factor (Fig. 8a) shows maximum concentrations persisting
620 throughout the night and early morning, while a secondary maximum during the midday can be observed. But overall, the

621 diurnal pattern of LO-OOA is rather flat compared to the cold period, suggesting that local production may not be so important
 622 at that time compared to a less variable regional background. Interestingly a midday hump similar to the one observed for
 623 HOA-2 is present, suggesting a common origin.

624 **MO-OOA:** The factor profile of MO-OOA resolved during the warm period is strikingly identical to the profile found in the
 625 cold period (their R^2 is almost 1; Fig. S10e), while being excellently correlated to other highly oxygenated OA factors resolved
 626 in both the urban and regional background in the Eastern Mediterranean (Bougiatioti et al., 2014; Stavroulas et al., 2019, 2021)
 627 as well as in continental Europe (Crippa et al., 2014). The winter night-time peaks are not observed anymore (Fig. 8a), with
 628 the factor's diurnal pattern exhibiting much less variability, highlighting its dominant regional character. The time series of
 629 MO-OOA correlates ~~good~~ well to SO_4^{2-} ($R^2=0.53$; $N=1259$; Fig. S15b), confirming this regional and highly processed origin.
 630 The concentration levels of MO-OOA during the warm period are lower than in the cold (Table S32). However, its relative
 631 contribution to total OA during the warm period remains similar (45 %).

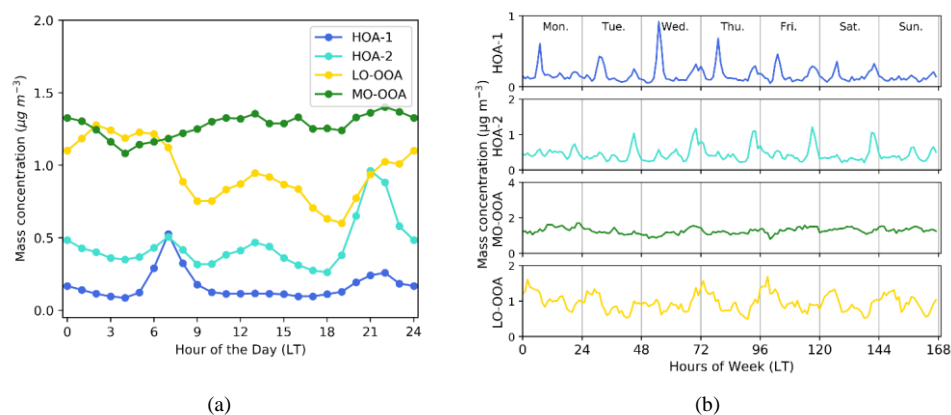


632

- Formatted Table
- Formatted: Centered
- Formatted: Caption

633

634 **Figure 7: Mass spectra of the PMF (a) and the time series of the four OA factors resolved along with corresponding tracer**
 635 **compounds (b) for the warm period.**



636 **Figure 8: Diurnal variability (a) and weekly cycles (b) of the four OA factors resolved during the warm period.**

637 3.6. Spatial and seasonal variability of OA sources

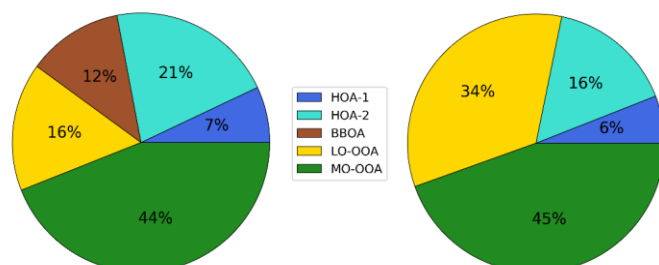
638 3.6.1. Seasonal variability of OA sources

639 **Primary OA:** The mass concentration of the three primary OA factors (HOA-1, HOA-2, BBOA) represents as much as 40 %
 640 of total organic aerosols during the cold period (Fig. 9), with POA contribution significantly decreasing in the warm period
 641 (22% to total OA) due to the absence of the significant residential wood burning source which during the cold period accounted
 642 for 12% of total OA. The important contribution of primary sources in Nicosia has been also been highlighted earlier, by the
 643 rather low OA/OC ratio of 1.42 (Section 3.1). In a recent publication covering several European sites, Chen et al. (2022)
 644 reported that in urban sites, solid fuel combustion-related OA components were 21.4 % of total OA during winter months,
 645 higher than what is found for BBOA in Nicosia, owing to the rather milder winters in the city.

646 The traffic-related primary factor in Nicosia (HOA-1) was found to be rather stable in terms of contribution to total OA across
 647 this study's two seasons, averaging 7% and 6%, respectively, for the cold and warm periods, being lower than the figure
 648 reported in other European Urban sites (12.7%, Chen et al., 2022). On the other hand, the HOA-2 factor represents ca 2/3 of
 649 the total HOA in Nicosia with little variation from winter (72 %) to summer (66 %) to total HOA (Fig. 9). Comparing it with
 650 COA in urban locations resolved by Chen et al. (2022), during both winter (14.4% compared to 21% in the cold season in
 651 Nicosia) and spring (15% versus 16% in Nicosia during the warm season), the higher values reported in Nicosia further support
 652 the assumption that the HOA-2 represents a mixed combustion source.

653 **Secondary OA:** A higher degree of oxidation is observed for the LO-OOA factor during the warm period, given the much
 654 higher contribution of signal contribution at m/z 44 compared to than the respective cold period factor. This discrepancy,
 655 reported in several studies (Huang et al., 2019; Duan et al., 2020), is explained by higher photochemistry during the warm
 656 period, which promotes the oxidation of OA, resulting in an LO-OOA profile with a higher m/z 44 fraction. This result is also
 657 consistent with a less-oxidized LO-OOA formed during the cold period from night-time chemistry. The range of LO-OOA
 658 concentration levels are is different between cold and warm periods (0.05-7.74 $\mu\text{g m}^{-3}$ and 0.05-4.00 $\mu\text{g m}^{-3}$, respectively),
 659 while the mean concentrations for both periods are similar (0.86 and 0.95 $\mu\text{g m}^{-3}$ for cold and warm periods respectively). The
 660 contribution of LO-OOA relative to total OA is double during the warm period compared to the cold, reflecting both the
 661 absence of the biomass burning source as well as the prevailing conditions favoring atmospheric processing of primary OA
 662 and SOA precursors. During the cold period, LO-OOA intense peaks suggest an influence from local emissions, while during
 663 the warm period, the less-variable LO-OOA diurnal variability highlights the influence of more intense photochemical
 664 processing at medium-to-large geographical scale. MO-OOA is found to be the major contributor to total OA for both the cold

665 (44%) and warm (45%) periods, higher in both cases than the average MO-OOA contributions reported for other European
 666 urban sites (Chen et al., 2022) underlining the importance of highly processed secondary OA over Nicosia (Fig. 9).



667
 668 **Figure 9: Relative contribution of PMF resolved OA sources to total OA for the cold period (left) and the warm period (right),**
 669 **respectively.**

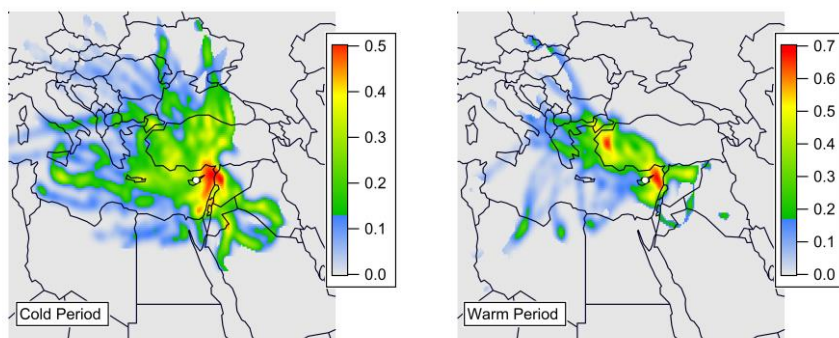
670 3.6.2. Geographic origin of OA sources

671 The geographic origin of OA sources (local vs regional) is further assessed here using both Non-parametric Wind Regression
 672 (NWR) analyses as well as the regional scale coupling concentrations to air mass back trajectories through PSCF.

673 **Cold period:** During this period, primary OA factors, especially HOA-1 and BBOA, have an expected strong local component
 674 that is characterized by high concentrations at low wind speeds (hourly average 1.4 m s^{-1}) when winds are originating from the
 675 W-SW sector (Fig. S14a,c), pointing to the busy highway connecting Nicosia to the other major cities in the island while
 676 integrating the highly populated residential areas of Strovolos and Lakatamia municipalities. (Fig. 1c). As discussed earlier,
 677 the HOA-2 factor, apart from its local influence (also in the W-SW sector), exhibits significant concentrations related to higher
 678 wind speeds from the NW and the E-NE sectors that could originate from power plants but also possibly from long-range
 679 transport. Interestingly, a small local contribution from the city, still within the W-SW sector, can ~~be also~~ be observed for
 680 both LO-OOA and MO-OOA, consistent with the peaks observed that could originate from local night-time chemistry. Still,
 681 high concentrations of MO-OOA (and, to a lesser extent LO-OOA) are observed with high wind speeds and Eastern directions
 682 (Fig. S14e,d). Although the contribution of the power plant PP5 located in the East sector (Fig. S13c) cannot be excluded,
 683 PSCF analysis points out that the hotspots of MO-OOA can be traced in neighbouring countries (eg. Syria, Lebanon ~~and~~ South
 684 Turkey) in the middle East (Fig 10a). These areas also represent hotspots of SO_4^{2-} according to PSCF analysis (Fig. S17a).

685 **Warm period:** Given the generally higher wind speeds recorded, in comparison to the cold season (average of 1.93 m s^{-1} vs.
 686 1.36 m s^{-1} in the cold period), all OA factors show elevated concentrations coupled with higher wind speeds. The most striking
 687 result is the major influence of the E-SE sector for all OA sources. ~~However, although~~ this sector is upwind of Nicosia and,
 688 therefore, poorly influenced by local city emissions. As noted previously, for the cold period, long-range transported OA from
 689 the Middle East is expected to be the main driver ~~here~~ to explain the influence of the E-SE sector, at least for LO-OOA and
 690 MO-OOA (Fig. S16c,d). This is ~~once~~ again confirmed ~~from~~ by the PSCF results reported in Fig. 10b for the warm period. The
 691 HOA-1 factor still shows maxima for low wind speeds ($<5 \text{ km h}^{-1}$) characteristic of local emissions and the SW-S direction,
 692 but also exhibits significant contribution related to the E-SE sector. Although the influence of the power plant PP5 on HOA-2
 693 is expected, ~~the~~ contribution of this source can not be excluded for HOA-1 as well. On the other hand, quantification of the
 694 Middle Eastern contribution to the HOA-2 factor remains to be assessed; since the current dataset cannot provide sufficient
 695 information on separating the contribution of power plants on the island versus more regional Middle East emissions (Fig.
 696 S165b). Although this hypothesis needs further investigation, the presence of HOA-2 in the Middle East would be consistent
 697 with recent findings highlighting the importance of OC emissions from diesel generators used in Lebanon as a means of
 698 complementary power generation (Fadel et al., 2022).

699



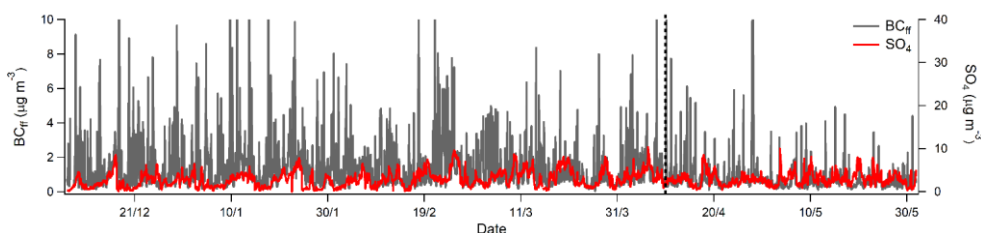
701 **Figure 10: PSCF plots for MO-OOA during the cold and warm periods.** Color scale represents the probability of air
 702 parcels arriving at the receptor site (white dot) for measured concentrations higher than the 75th percentile PSCF values while the
 703 sampling site is denoted with a white dot.

Formatted: Superscript

704 In conclusion, based on the relative contribution of OA factors (Fig. 9) and the NWR analysis (Fig. S14, S16), it can be
 705 reasonably assumed that a significant amount of measured OA in Nicosia is originating/originates from long-range transport
 706 with the Middle East being the major source region, during both cold and warm periods. This is the first time that such a high
 707 contribution of OA from the Middle East is highlighted over Cyprus. Assuming that biomass combustion and biogenic
 708 emissions of OA in the desert regions of the Middle East are relatively limited, these results suggest that most of the primary
 709 and secondary OA originating from the Middle East could be of fossil fuel origin, which is consistent with the previously
 710 reported large-extensive use of oil in this region.

711 3.7. Spatial and seasonal variability of BC sources

712 The above conclusion on the influence of primary and secondary OA sources from the Middle East region, and its strong fossil
 713 fuel origin, motivates a careful examination of the geographic origin and sources of BC concentrations recorded in Nicosia.
 714 Baseline (i.e., lowest) BC_{ff} concentrations are typically observed in the middle of the night and in the middle of the day, when
 715 local emissions are at their minimum (See Fig. 4). As such, these background concentrations can be considered as a first
 716 qualitative indicator of background BC_{ff} concentrations of regional origin. Interestingly, these baseline BC_{ff} concentrations
 717 appear to be in phase with those of sulphate-sulfate (Fig. 11), as well as the MO-OOA factor derived from the OA PMF
 718 analysis. This observation points to the possible use of MO-OOA as a tracer for regional BC_{ff}. Hence, it brings further evidence
 719 on-of the importance of regional emissions on carbonaceous aerosol concentrations in Nicosia.



720 **Figure 11: Temporal variability of BC_{ff} and SO₄²⁻ concentrations during the entire measuring periods.**

721 The assumption that transported regional pollution can affect BC_{ff} concentrations in Nicosia can be further supported by
 722 investigating the BC_{ff} NWR polar plots for both the cold and warm seasons (Fig. S18a,b). Elevated concentrations related to

723 local emissions were observed for calm conditions with low wind speeds ($<5 \text{ km h}^{-1}$) in the SW sector, as previously observed
724 for HOA-1. Interestingly, BC_{ff} NWR plots show a distinct contribution at higher wind speeds ($\sim 15 \text{ km h}^{-1}$) and the NE-SE
725 (Middle East) sector, during both the cold and warm periods, with estimated concentrations of roughly $1.5 \mu\text{g m}^{-3}$, further
726 support the major role of the Middle East in the observed BC concentration levels in Nicosia (Fig S18 a,b).

727 BC source apportionment: In order to better assess the relative contributions of the multiple primary OA sources (HOA-1,
728 HOA-2) and to quantify the contribution of long-range transport from the Middle East to BC_{ff} , a multilinear regression (MLR)
729 model was tentatively performed using the principle of co-emission of BC_{ff} and organic species by the different sources
730 (Chirico et al., 2010; Laborde et al., 2013). This approach, used recently by Poulain et al. (2021), assumes that at any given
731 time (t), BC_{ff} mass concentration is the sum of BC from traffic (traced by HOA-1), from a mixed combustion source (traced
732 by HOA-2), and from long-range transport (traced by MO-OOA), as follows:

$$[\text{BC}]_{\text{ff}} = [\text{BC}]_{\text{traffic}} + [\text{BC}]_{\text{mix combustion}} + [\text{BC}]_{\text{regional}} \quad (2)$$

734 With:

$$[\text{BC}]_{\text{traffic}} = a \times [\text{HOA-1}] \quad (3)$$

$$[\text{BC}]_{\text{mix combustion}} = b \times [\text{HOA-2}] \quad (4)$$

$$[\text{BC}]_{\text{regional}} = c \times [\text{MO-OOA}] \quad (5)$$

738 Where a, b, and c are coefficients derived from the multi-linear regression model.

739 The above approach assumes that primary HOA-1 and HOA-2 can trace $\text{BC}_{\text{traffic}}$ and $\text{BC}_{\text{mix combustion}}$, respectively. This is
740 somewhat expected for traffic which with has a typical HOA-1/ $\text{BC}_{\text{traffic}}$ ratio with little variations. For HOA-2, this assumption
741 is valid for the fraction that is assumed to originate from power plant emissions, and for some of the cooking activities (e.g.,
742 when using charcoal combustion) but not necessarily all. As such, the uncertainties of this approach is are expected to be
743 higher for HOA-2, compared to HOA-1. The use of MO-OOA to trace the regional source of BC would probably lead to even
744 higher uncertainties due to the fact that because MO-OOA is also sensitive to atmospheric photochemical processes and does
745 integrate multiple sources. Nevertheless, this latter assumption is believed to be acceptable given the good agreement reported
746 above between baseline concentrations of BC_{ff} and MO-OOA (Fig. S19); and the above conclusions that carbonaceous aerosols
747 originating from the Middle East are expected to be dominated by fossil fuel combustion. Note that MO-OOA was preferred
748 here to LO-OOA to trace regional emissions due to the latter's somewhat more local character.

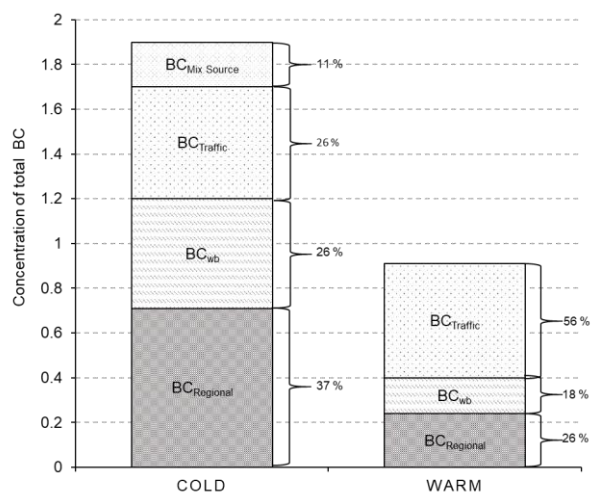
749 Combining equations 2-5 provides the multilinear regression model with the free regression parameters a, b, c, which are fitted
750 to the time-resolved BC_{ff} mass concentration measured by the Aethalometer and PMF results for the ACSM data:

$$[\text{BC}]_{\text{ff}} = a \times [\text{HOA-1}] + b \times [\text{HOA-2}] + c \times [\text{MO-OOA}] \quad (6)$$

752 Previous studies have shown that MLR models seem to have enhanced explanatory power when primary emissions are
753 dominant/dominate (Laborde et al., 2013). To reduce this potential bias, the MLR model was applied distinctly for the two
754 seasons separately.

755 During the cold period, a very good correlation between measured and modelled BC_{ff} was obtained ($r^2 = 0.70$; $N = 2942$), with
756 the modelled BC_{ff} explaining 84 % of the measured one (Fig. S20a). The regression coefficients a (HOA-1), b (HOA-2) and
757 c (MO-OOA) were found to be 1.11 ± 0.03 , 0.15 ± 0.01 and 0.41 ± 0.01 , respectively. Regarding the warm period, it was not
758 possible to obtain a positive value for b (HOA-2). A correlation between long-range transported HOA-2 and MO-OOA is,
759 among other, a reason that can be proposed to explain why it has not been possible to extract a $\text{BC}_{\text{mix source}}$ factor here. Therefore,
760 BC_{ff} was only apportioned using HOA-1 and MO-OOA. A good correlation between measured and modelled BC_{ff} was
761 obtained ($r^2=0.62$; $N=1251$), with the modelled BC_{ff} , explaining 83% of observations (Fig S20b). The regression coefficients
762 a (HOA-1) and c (MO-OOA) were found to be 3.05 ± 0.07 and 0.19 ± 0.01 , respectively.

763 The combination of the Aethalometer model (apportioning BC_{ff} and BC_{wb}) and the MLR model (apportioning $\text{BC}_{\text{traffic}}$, BC_{mix}
764 source, and $\text{BC}_{\text{regional}}$) was performed to obtain an integrated picture of BC sources in Nicosia for both periods (see Fig. 12).



765

766 **Figure 12:** BC sources during the cold and the warm period in Nicosia

767 **Spatial and seasonal variability of BC sources:** During the cold period, BC was found to originate from four different sources
 768 denoting the complexity of combustion sources of different origins in Nicosia. BC_{regional} is the dominant source of BC (37%),
 769 while traffic, wood burning, and mix source are estimated to contribute to 26 %, 26% and 11% of BC, respectively. From the
 770 perspective of BC_{ff} sources, long-range transport, traced by MO-OOA, remains the largest source of BC_{ff} during the cold
 771 period, contributing 63 %, while BC_{ff} from local emissions constrained with HOA-1 and HOA-2 represents 24% and 13%,
 772 respectively (Fig S21). In other words, more than half of BC_{ff} in Nicosia was found to be regional and **most probably**
 773 **originating probably originated** from the Middle East during the cold period. This high contribution of regional BC_{ff} is quite
 774 unexpected for a medium-sized European city like Nicosia, where local traffic is likely to be the main contributor to BC_{ff}.
 775 Nevertheless, extra caution should be taken here, ~~and t~~the obtained contribution of 63% for BC_{ff} regional should be seen as
 776 an upper limit since a fraction of MO-OOA was shown to be of local origin during the cold period. During the warm period,
 777 the picture remains similar, with traffic and wood burning- representing two-thirds of BC (56 % & 18 %). Here, BC regional
 778 contributed 26 % to total BC. From the perspective of BC_{ff} sources during **the** warm period, the long-range transport,
 779 contributed 41 %, while BC_{ff} from local emissions constrained with HOA-1 represents 59 % (Fig S21). Although the two
 780 models (Aethalometer and MLR) are associated with non-negligible uncertainties, the BC source apportionment obtained,
 781 shows that local emissions cannot be considered only for BC, with demonstrated significant contribution of Middle East fossil
 782 fuel emissions.

783 4. Conclusions

784 Near-real-time chemical composition of submicron aerosols and source apportionment of carbonaceous aerosols was
 785 performed for the first time in Nicosia, a medium-sized European capital city (circa 250,000 inhabitants) in Cyprus located in
 786 the Eastern Mediterranean and surrounded by Middle East countries with fast-growing population and increasing emissions
 787 of air pollutants. Continuous observations were performed at an urban background site, for approximately 6 months (between
 788 7 December 2018 and 31 May 2019); in order to obtain a large and representative dataset capturing specific features related
 789 to **both the** cold and warm periods, such as domestic heating and regional transport. Measurements of the major fractions of
 790 PM₁ were carried out with a Q-ACSM and an Aethalometer complemented by a comprehensive suite of collocated instruments
 791 (e.g., filter sampling, SMPS) to **further** assess the quality of the acquired data **further**.

792 Unlike many European cities, no clear PM₁ pollution episodes of several consecutive days could be observed over Nicosia.
793 However, very intense peaks (above 40 µg m⁻³ 1h averages) were recorded systematically every evening during the cold
794 period. Carbonaceous aerosols (BC and OA) were identified as the main components of these peaks and were mostly attributed
795 to local emissions from heating with ~~only~~ little contribution from local meteorology (PBL height did not show significant
796 diurnal variability during the cold period). ~~Furthermore, a significant portion of PM₁ was found to be related to long range~~
797 ~~transported aerosol, while the influence of shipping emissions was estimated to be rather low (less than 8%).~~
798 Source apportionment of OA has been used to derive a local biomass burning OA (BBOA_{cy}) mass spectrum, in order to
799 ~~properly~~ apportion the contribution of domestic wood burning ~~properly~~. A total of five OA sources were identified during the
800 cold period, among which four are typically reported within urban environments (HOA-1, BBOA, LO-OOA, MO-OOA). An
801 additional one (HOA-2) was assigned as a mixture of several combustion sources, such as cooking as well as a significant
802 contribution from power plants located in the Northern part of the island. These power plants in addition, represent major
803 island-based hotspots of NO_x, as evidenced ~~from~~ ~~by~~ satellite observations. Interestingly, a similar HOA-2 source was identified
804 at our regional background site (40 km distance from Nicosia; Chen et al., 2022), pointing to a possible influence from these
805 power plants to an extended part of the island. The impact of this specific source brings the OA contribution of primary sources
806 up to 40 % over Nicosia during the cold period. Few additional features were noticed for the other OA sources with 1) a typical
807 traffic-related (HOA-1) source observed during both seasons, 2) a biomass burning source (BBOA) related to domestic heating
808 enhanced at night during the cold season and accounting for 12 % of the total OA, 3) a less oxidized secondary (LO-OOA)
809 source of a semi-volatile character, ~~and~~ influenced by local night-time chemistry, that ~~shows waste to be~~ more oxidized (~~and i.e.,~~
810 ~~of a more regional originless local character~~) during the warm period, and 4) a secondary (MO-OOA) source mostly of regional
811 origin but also influenced by night-time chemistry during the cold period.
812 The geographic origin of each OA source was assessed for both seasons. ~~With the exception of~~ ~~Except for~~ MO-OOA, which
813 ~~shows~~ systematically ~~shows~~ a strong regional component, HOA-1, HOA-2, and LO-OOA exhibit a clear local origin during
814 both seasons, and a more pronounced influence from the Eastern wind sector during the warm period. The prevalence of this
815 sector is systematically observed for MO-OOA highlighting the major role of Middle East emissions in contributing to
816 ~~almost~~ half of OA concentrations in Nicosia during both cold and warm seasons.
817 To further elucidate the influence of this complex mixture of OA sources on BC levels, ~~a~~ source apportionment of BC was
818 performed ~~by~~ combining i) the aethalometer model to separate BC into its fossil fuel (BC_{ff}) and wood burning components
819 (BC_{wb}), and ii) a multi-linear regression model to apportion the contribution to BC_{ff} from traffic (constrained by HOA-1), mix
820 combustion sources from cooking and power plants (constrained by HOA-2), and long-range transport from the Middle East
821 (constrained by MO-OOA). Although several assumptions and uncertainties are associated with this approach, it has shown to
822 provide an interesting tool ~~to reconstruct~~ ~~for reconstructing~~ the BC concentrations derived experimentally. Such BC
823 apportionment performed for both cold and warm seasons solidified the conclusions reached through the OA source
824 apportionment, with almost half of BC_{ff} being of regional origin, with the Middle East playing an important role. This result
825 is quite unexpected given that local traffic emissions are usually considered the dominant contributor to BC_{ff} in urban
826 background environments. These conclusions have numerous implications related to PM regulation and the efficiency of local
827 abatement strategies (in particular regarding traffic emissions), health (combustion aerosols being considered as particularly
828 adverse for human health), and climate (major influence of light-absorbing aerosols from ~~the~~ Middle East fossil fuel
829 emissions).
830 More accurate OA and BC source apportionment i) with more co-located high-resolution measurements of specific trace metal
831 and organic tracers, ii) better resolved OA mass spectra (e.g., from HR-ToF-AMS), iii) the use of various source-specific mass
832 spectra fingerprints (e.g., from cooking or power plants), and iv) multi-site measurements (incl. both urban and regional
833 background) will enable a more accurate estimation of local vs. regional fossil fuel emissions in Cyprus while better
834 constraining the current regional efforts on air quality modelling and forecasting.

835

836 Data availability: All data used in this study can be accessed here:

837 <https://doi.org/10.5281/zenodo.7802065><https://doi.org/10.5281/zenodo.7186341>. More details on the analyses are available

838 upon request to the contact author Alikı Christodoulou (a.christodoulou@cyi.ac.cy).

839

840 Author contributions. AC, IS, MP, PG, KO, EB, [JK](#), RSE, MI, and MR contributed to the acquisition of measurements. AC,

841 IS contributed to the processing of the data. AC, IS, and JS wrote the manuscript. MV, NM, MD, SS, [and](#) MP -contributed to

842 the scientific review and improvement of the manuscript. All authors have read and agreed to the published version of the

843 manuscript

844

845 Acknowledgements.

846 This paper contains modified Copernicus Sentinel data processed at IUP Bremen. The authors thank Andreas Richter for

847 providing the TROPOMI/S5P level 1 and ~~level-2~~ products. This study has been co-funded by the European Union's Horizon

848 2020 research and innovation programme under grant agreement No 615 856612 (EMME-CARE); and by the Norwegian

849 Financial Mechanism and the Republic of Cyprus under the ACCEPT project (CY-LOCALDEV-0008) in the framework of

850 the programming period 2014 – 2021.

851

852 Competing interests. The authors declare that they have no conflict of interest. At the time of the research, Matic Ivančić and

853 Martin Rigler were employed by the manufacturer of the Aethalometer.

854

855 **References**

- 856 Achilleos, S., Evans, J. S., Yiallourou, P. K., Kleanthous, S., Schwartz, J., and Koutrakis, P.: PM10 concentration levels at an
857 urban and background site in Cyprus: The impact of urban sources and dust storms, *J. Air Waste Manag. Assoc.*, 64, 1352–
858 1360, <https://doi.org/10.1080/10962247.2014.923061>, 2014.
- 859 Achilleos, S., Wolfson, J. M., Ferguson, S. T., Kang, C. M., Hadjimitsis, D. G., Hadjicharalambous, M., Achilleos, C.,
860 Christodoulou, A., Nisanzi, A., Papoutsas, C., Themistocleous, K., Athanasatos, S., Perdikou, S., and Koutrakis, P.: Spatial
861 variability of fine and coarse particle composition and sources in Cyprus, *Atmos. Res.*, 169, 255–270,
862 <https://doi.org/10.1016/j.atmosres.2015.10.005>, 2016.
- 863 Aiken, A. C., Decarlo, P. F., Kroll, J. H., Worsnop, D. R., Huffman, J. A., Docherty, K. S., Ulbrich, I. M., Mohr, C., Kimmel,
864 J. R., Sueper, D., Sun, Y., Zhang, Q., Trimborn, A., Northway, M., Ziemann, P. J., Canagaratna, M. R., Onasch, T. B., Alfarra,
865 M. R., Prevot, A. S. H., Dommen, J., Duplissy, J., Metzger, A., Baltensperger, U., and Jimenez, J. L.: O/C and OM/OC ratios
866 of primary, secondary, and ambient organic aerosols with high-resolution time-of-flight aerosol mass spectrometry, *Environ.*
867 *Sci. Technol.*, 42, 4478–4485, <https://doi.org/10.1021/es703009q>, 2008.
- 868 Ait-Helal, W., Borbon, A., Sauvage, S., De Gouw, J. A., Colomb, A., Gros, V., Freutel, F., Crippa, M., Afif, C., Baltensperger,
869 U., Beekmann, M., Doussin, J. F., Durand-Jolibois, R., Fronval, I., Grand, N., Leonardis, T., Lopez, M., Michoud, V., Miet,
870 K., Perrier, S., Prévôt, A. S. H., Schneider, J., Siour, G., Zapf, P., and Locoge, N.: Volatile and intermediate volatility organic
871 compounds in suburban Paris: Variability, origin and importance for SOA formation, *Atmos. Chem. Phys.*, 14, 10439–10464,
872 <https://doi.org/10.5194/acp-14-10439-2014>, 2014.
- 873 Alfarra, M. R., Prevot, A. S. H., Szidat, S., Sandradewi, J., Weimer, S., Lanz, V. A., Schreiber, D., Mohr, M., and
874 Baltensperger, U.: Identification of the mass spectral signature of organic aerosols from wood burning emissions, *Environ.*
875 *Sci. Technol.*, 41, 5770–5777, <https://doi.org/10.1021/es062289b>, 2007.
- 876 Basart, S., Pérez, C., Cuevas, E., Baldasano, J. M., and Gobbi, G. P.: Aerosol characterization in Northern Africa, Northeastern
877 Atlantic, mediterranean basin and middle east from direct-sun AERONET observations, *Atmos. Chem. Phys.*, 9, 8265–8282,
878 <https://doi.org/10.5194/acp-9-8265-2009>, 2009.
- 879 Berger, A., Barbet, C., Leriche, M., Deguillaume, L., Mari, C., Bègue, N., Tulet, P., Gazen, D., Escobar, J., Berger, A., Barbet,
880 C., Leriche, M., Deguillaume, L., and Mari, C.: Evaluation of Meso-NH and WRF / CHEM simulated gas and aerosol
881 chemistry over Europe based on hourly observations To cite this version : HAL Id : hal-01307985 Evaluation of Meso - NH
882 and WRF / CHEM simulated gas and aerosol chemistry over Europe based on , 2016.
- 883 Bougiatioti, A., Stavroulas, I., Kostenidou, E., Zarnmpas, P., Theodosi, C., Kouvarakis, G., Canonaco, F., Prévôt, A. S. H.,
884 Nenes, A., Pandis, S. N., and Mihalopoulos, N.: Processing of biomass-burning aerosol in the eastern Mediterranean during
885 summertime, *Atmos. Chem. Phys.*, 14, 4793–4807, <https://doi.org/10.5194/acp-14-4793-2014>, 2014.
- 886 Bressi, M., Cavalli, F., Belis, C. A., Putaud, J. P., Fröhlich, R., Martins Dos Santos, S., Petralia, E., Prévôt, A. S. H., Berico,
887 M., Malaguti, A., and Canonaco, F.: Variations in the chemical composition of the submicron aerosol and in the sources of the
888 organic fraction at a regional background site of the Po Valley (Italy), *Atmos. Chem. Phys.*, 16, 12875–12896,
889 <https://doi.org/10.5194/acp-16-12875-2016>, 2016.
- 890 Bressi, M., Cavalli, F., Putaud, J. P., Fröhlich, R., Petit, J. E., Aas, W., Äijälä, M., Alastuey, A., Allan, J. D., Aurela, M.,
891 Berico, M., Bougiatioti, A., Bukowiecki, N., Canonaco, F., Crenn, V., Dusanter, S., Ehn, M., Elsasser, M., Flentje, H., Graf,
892 P., Green, D. C., Heikkinen, L., Hermann, H., Holzinger, R., Hueglin, C., Keernik, H., Kiendler-Scharr, A., Kubelová, L.,
893 Lunder, C., Maasikmets, M., Makeš, O., Malaguti, A., Mihalopoulos, N., Nicolas, J. B., O'Dowd, C., Ovadnevaite, J., Petralia,
894 E., Poulain, L., Priestman, M., Riffault, V., Ripoll, A., Schlag, P., Schwarz, J., Sciare, J., Slowik, J., Sosedova, Y., Stavroulas,
895 I., Teinmaa, E., Via, M., Vodička, P., Williams, P. I., Wiedensohler, A., Young, D. E., Zhang, S., Favez, O., Minguillón, M.
896 C., and Prevot, A. S. H.: A European aerosol phenomenology - 7: High-time resolution chemical characteristics of submicron
897 particulate matter across Europe, *Atmos. Environ. X*, 10, <https://doi.org/10.1016/j.aeoa.2021.100108>, 2021.
- 898 Brown, S. G., Lee, T., Roberts, P. T., and Collett, J. L.: Variations in the OM/OC ratio of urban organic aerosol next to a major
899 roadway, *J. Air Waste Manag. Assoc.*, 63, 1422–1433, <https://doi.org/10.1080/10962247.2013.826602>, 2013.
- 900 Canonaco, F., Crippa, M., Slowik, J. G., Baltensperger, U., and Prévôt, A. S. H.: SoFi, an IGOR-based interface for the efficient

901 use of the generalized multilinear engine (ME-2) for the source apportionment: ME-2 application to aerosol mass spectrometer
902 data, *Atmos. Meas. Tech.*, 6, 3649–3661, <https://doi.org/10.5194/amt-6-3649-2013>, 2013.

903 Canonaco, F., Slowik, J. G., Baltensperger, U., and Prévôt, A. S. H.: Seasonal differences in oxygenated organic aerosol
904 composition: Implications for emissions sources and factor analysis, *Atmos. Chem. Phys.*, 15, 6993–7002,
905 <https://doi.org/10.5194/acp-15-6993-2015>, 2015.

906 Cavalli, F. and Pataud, J. P.: Toward a standardized thermal-optical protocol for measuring atmospheric organic and elemental
907 carbon: The eusaar protocol, *ACS, Div. Environ. Chem. - Prepr. Ext. Abstr.*, 48, 443–446, 2008.

908 Chazeau, B., Temime-Roussel, B., Gille, G., Mesbah, B., D’Anna, B., Wortham, H., and Marchand, N.: Measurement report:
909 Fourteen months of real-time characterisation of the submicronic aerosol and its atmospheric dynamics at the Marseille-
910 Longchamp supersite, *Atmos. Chem. Phys.*, 21, 7293–7319, <https://doi.org/10.5194/acp-21-7293-2021>, 2021.

911 Chen, G., Sosedova, Y., Canonaco, F., Fröhlich, R., Tobler, A., Vlachou, A., Daellenbach, K. R., Bozzetti, C., Hueglin, C.,
912 Graf, P., Baltensperger, U., Slowik, J. G., El Haddad, I., and Prévôt, A. S. H.: Time-dependent source apportionment of
913 submicron organic aerosol for a rural site in an alpine valley using a rolling positive matrix factorisation (PMF) window,
914 *Atmos. Chem. Phys.*, 21, 15081–15101, <https://doi.org/10.5194/acp-21-15081-2021>, 2021.

915 Chen, G., Canonaco, F., Tobler, A., Aas, W., Alastuey, A., Allan, J., Atabakhsh, S., Aurela, M., Baltensperger, U., Bougiatioti,
916 A., De Brito, J. F., Ceburnis, D., Chazeau, B., Chebaicheb, H., Daellenbach, K. R., Ehn, M., El Haddad, I., Eleftheriadis, K.,
917 Favez, O., Flentje, H., Font, A., Fossum, K., Freney, E., Gini, M., Green, D. C., Heikkinen, L., Herrmann, H., Kalogridis, A.
918 C., Keernik, H., Lhotka, R., Lin, C., Lunder, C., Maasikmets, M., Manousakas, M. I., Marchand, N., Marin, C., Marmureanu,
919 L., Mihalopoulos, N., Močnik, G., Nećki, J., O’Dowd, C., Ovadnevaite, J., Peter, T., Petit, J. E., Pikridas, M., Matthew Platt,
920 S., Pokorná, P., Poulain, L., Priestman, M., Riffault, V., Rinaldi, M., Róžański, K., Schwarz, J., Sciare, J., Simon, L., Skiba,
921 A., Slowik, J. G., Sosedova, Y., Stavroulas, I., Styszko, K., Teinemia, E., Timonen, H., Tremper, A., Vasilescu, J., Via, M.,
922 Vodička, P., Wiedensohler, A., Zografou, O., Cruz Minguillón, M., and Prévôt, A. S. H.: European aerosol phenomenology –
923 8: Harmonised source apportionment of organic aerosol using 22 Year-long ACSM/AMS datasets, *Environ. Int.*, 166,
924 <https://doi.org/10.1016/j.envint.2022.107325>, 2022.

925 Chin, M., Diehl, T., Tan, Q., Prospero, J. M., Kahn, R. A., Remer, L. A., Yu, H., Sayer, A. M., Bian, H., Geogdzhayev, I. V.,
926 Holben, B. N., Howell, S. G., Huebert, B. J., Hsu, N. C., Kim, D., Kucsera, T. L., Levy, R. C., Mishchenko, M. I., Pan, X.,
927 Quinn, P. K., Schuster, G. L., Streets, D. G., Strode, S. A., and Torres, O.: Multi-decadal aerosol variations from 1980 to 2009:
928 A perspective from observations and a global model, *Atmos. Chem. Phys.*, 14, 3657–3690, <https://doi.org/10.5194/acp-14-3657-2014>, 2014.

930 Chirico, R., Decarlo, P. F., Heringa, M. F., Tritscher, T., Richter, R., Prévôt, A. S. H., Dommen, J., Weingartner, E., Wehrle,
931 G., Gysel, M., Laborde, M., and Baltensperger, U.: Impact of aftertreatment devices on primary emissions and secondary
932 organic aerosol formation potential from in-use diesel vehicles: Results from smog chamber experiments, *Atmos. Chem. Phys.*,
933 10, 11545–11563, <https://doi.org/10.5194/acp-10-11545-2010>, 2010.

934 Crenn, V., Sciare, J., Croteau, P. L., Verlhac, S., Fröhlich, R., Belis, C. A., Aas, W., Äijälä, M., Alastuey, A., Artiñano, B.,
935 Baisnée, D., Bonnaire, N., Bressi, M., Canagaratna, M., Canonaco, F., Carbone, C., Cavalli, F., Coz, E., Cubison, M. J., Esser-
936 Gietl, J. K., Green, D. C., Gros, V., Heikkinen, L., Herrmann, H., Lunder, C., Minguillón, M. C., Močnik, G., O’Dowd, C. D.,
937 Ovadnevaite, J., Petit, J. E., Petralia, E., Poulain, L., Priestman, M., Riffault, V., Ripoll, A., Sarda-Estève, R., Slowik, J. G.,
938 Setyan, A., Wiedensohler, A., Baltensperger, U., Prévôt, A. S. H., Jayne, J. T., and Favez, O.: ACTRIS ACSM intercomparison
939 - Part 1: Reproducibility of concentration and fragment results from 13 individual Quadrupole Aerosol Chemical Speciation
940 Monitors (Q-ACSM) and consistency with co-located instruments, *Atmos. Meas. Tech.*, 8, 5063–5087,
941 <https://doi.org/10.5194/amt-8-5063-2015>, 2015.

942 Crippa, M., Canonaco, F., Lanz, V. A., Äijälä, M., Allan, J. D., Carbone, S., Capes, G., Ceburnis, D., Dall’Osto, M., Day, D.
943 A., DeCarlo, P. F., Ehn, M., Eriksson, A., Freney, E., Ruiz, L. H., Hillamo, R., Jimenez, J. L., Junninen, H., Kiendler-Scharr,
944 A., Kortelainen, A. M., Kulmala, M., Laaksonen, A., Mensah, A. A., Mohr, C., Nemitz, E., O’Dowd, C., Ovadnevaite, J.,
945 Pandis, S. N., Petäjä, T., Poulain, L., Saarikoski, S., Sellegri, K., Swietlicki, E., Tiitta, P., Worsnop, D. R., Baltensperger, U.,
946 and Prévôt, A. S. H.: Organic aerosol components derived from 25 AMS data sets across Europe using a consistent ME-2
947 based source apportionment approach, *Atmos. Chem. Phys.*, 14, 6159–6176, <https://doi.org/10.5194/acp-14-6159-2014>, 2014.

948 Cubison, M. J., Ortega, A. M., Hayes, P. L., Farmer, D. K., Day, D., Lechner, M. J., Brune, W. H., Apel, E., Diskin, G. S.,
949 Fisher, J. A., Fuelberg, H. E., Hecobian, A., Knapp, D. J., Mikoviny, T., Riemer, D., Sachse, G. W., Sessions, W., Weber, R.

- 950 J., Weinheimer, A. J., Wisthaler, A., and Jimenez, J. L.: Effects of aging on organic aerosol from open biomass burning smoke
951 in aircraft and laboratory studies, *Atmos. Chem. Phys.*, 11, 12049–12064, <https://doi.org/10.5194/acp-11-12049-2011>, 2011.
- 952 Debevec, C., Sauvage, S., Gros, V., Sciare, J., Pikridas, M., Stavroulas, I., Salameh, T., Leonaridis, T., Gaudion, V., Depelchin,
953 L., Fronval, I., Sarda-Esteve, R., Baisnée, D., Bonsang, B., Savvides, C., Vrekoussis, M., and Locoge, N.: Origin and variability
954 in volatile organic compounds observed at an Eastern Mediterranean background site (Cyprus), *Atmos. Chem. Phys.*, 17,
955 11355–11388, <https://doi.org/10.5194/acp-17-11355-2017>, 2017.
- 956 Drinovec, L., Močnik, G., Zotter, P., Prévôt, A. S. H., Ruckstuhl, C., Coz, E., Rupakheti, M., Sciare, J., Müller, T.,
957 Wiedensohler, A., and Hansen, A. D. A.: The “dual-spot” Aethalometer: An improved measurement of aerosol black carbon
958 with real-time loading compensation, *Atmos. Meas. Tech.*, 8, 1965–1979, <https://doi.org/10.5194/amt-8-1965-2015>, 2015.
- 959 Duan, J., Huang, R. J., Li, Y., Chen, Q., Zheng, Y., Chen, Y., Lin, C., Ni, H., Wang, M., Ovadnevaite, J., Ceburnis, D., Chen,
960 C., Worsnop, D. R., Hoffmann, T., O’Dowd, C., and Cao, J.: Summertime and wintertime atmospheric processes of secondary
961 aerosol in Beijing, *Atmos. Chem. Phys.*, 20, 3793–3807, <https://doi.org/10.5194/acp-20-3793-2020>, 2020.
- 962 Dulac, F. and Hamonou, E.: Chapter 4. Air quality and climate in the Mediterranean region, *Mediterr. Reg. under Clim. Chang.*
963 *A Sci. Updat. Abr. English/French Version*, 39–44, <https://doi.org/10.4000/books.irdeditions.24600>, 2018.
- 964 Eyring, V., Köhler, H. W., Van Aardenne, J., and Lauer, A.: Emissions from international shipping: 1. The last 50 years, *J.*
965 *Geophys. Res. D Atmos.*, 110, 171–182, <https://doi.org/10.1029/2004JD005619>, 2005.
- 966 Fadel, M., Ledoux, F., Seigneur, M., Oikonomou, K., Sciare, J., Courcot, D., and Afif, C.: Chemical profiles of PM_{2.5} emitted
967 from various anthropogenic sources of the Eastern Mediterranean: Cooking, wood burning, and diesel generators, *Environ.*
968 *Res.*, 211, <https://doi.org/10.1016/j.envres.2022.113032>, 2022.
- 969 Florou, K., Papanastasiou, D. K., Pikridas, M., Kaltsonoudis, C., Louvaris, E., Gkatzelis, G. I., Patoulias, D., Mihalopoulos,
970 N., and Pandis, S. N.: The contribution of wood burning and other pollution sources to wintertime organic aerosol levels in
971 two Greek cities, *Atmos. Chem. Phys.*, 17, 3145–3163, <https://doi.org/10.5194/acp-17-3145-2017>, 2017.
- 972 Foret, G., Michoud, V., Kotthaus, S., Petit, J.-E., Baudic, A., Siour, G., Kim, Y., Doussin, J.-F., Dupont, J.-C., Formenti, P.,
973 Gaimoz, C., Ghersi, V., Gratién, A., Gros, V., Jaffrezo, J.-L., Haeffelin, M., Kreitz, M., Ravetta, F., Sartelet, K., Simon, L.,
974 Té, Y., Uzu, G., Zhang, S., Favez, O., and Beekmann, M.: The December 2016 extreme weather and particulate matter
975 pollution episode in the Paris region (France), *Atmos. Environ.*, 291, 119386, <https://doi.org/10.1016/j.atmosenv.2022.119386>,
976 2022.
- 977 Fourtziou, L., Liakakou, E., Stavroulas, I., Theodosi, C., Zarnpas, P., Psiloglou, B., Sciare, J., Maggos, T., Bairachtari, K.,
978 Bougiatioti, A., Gerasopoulos, E., Sarda-Estève, R., Bonnaire, N., and Mihalopoulos, N.: Multi-tracer approach to characterize
979 domestic wood burning in Athens (Greece) during wintertime, *Atmos. Environ.*, 148, 89–101,
980 <https://doi.org/10.1016/j.atmosenv.2016.10.011>, 2017.
- 981 Freutel, F., Schneider, J., Drewnick, F., Von Der Weiden-Reinmüller, S. L., Crippa, M., Prévôt, A. S. H., Baltensperger, U.,
982 Poulain, L., Wiedensohler, A., Sciare, J., Sarda-Estève, R., Burkhardt, J. F., Eckhardt, S., Stohl, A., Gros, V., Colomb, A.,
983 Michoud, V., Doussin, J. F., Borbon, A., Haeffelin, M., Morille, Y., Beekmann, M., and Borrmann, S.: Aerosol particle
984 measurements at three stationary sites in the megacity of Paris during summer 2009: Meteorology and air mass origin dominate
985 aerosol particle composition and size distribution, *Atmos. Chem. Phys.*, 13, 933–959, <https://doi.org/10.5194/acp-13-933-2013>, 2013.
- 987 Giannadaki, D., Pozzer, A., and Lelieveld, J.: Modeled global effects of airborne desert dust on air quality and premature
988 mortality, *Atmos. Chem. Phys.*, 14, 957–968, <https://doi.org/10.5194/acp-14-957-2014>, 2014.
- 989 Giannakis, E., Kushta, J., Bruggeman, A., and Lelieveld, J.: Costs and benefits of agricultural ammonia emission abatement
990 options for compliance with European air quality regulations, *Environ. Sci. Eur.*, 31, [https://doi.org/10.1186/s12302-019-0275-](https://doi.org/10.1186/s12302-019-0275-0)
991 0, 2019.
- 992 Gilardoni, S., Massoli, P., Paglione, M., Giulianelli, L., Carbone, C., Rinaldi, M., Decesari, S., Sandrini, S., Costabile, F.,
993 Gobbi, G. P., Pietrogrande, M. C., Visentin, M., Scotto, F., Fuzzi, S., and Facchini, M. C.: Direct observation of aqueous

- 994 secondary organic aerosol from biomass-burning emissions, *Proc. Natl. Acad. Sci. U. S. A.*, 113, 10013–10018,
995 <https://doi.org/10.1073/pnas.1602212113>, 2016.
- 996 Gunthe, S. S., Liu, P., Panda, U., Raj, S. S., Sharma, A., Darbyshire, E., Reyes-Villegas, E., Allan, J., Chen, Y., Wang, X.,
997 Song, S., Pöhlker, M. L., Shi, L., Wang, Y., Kommula, S. M., Liu, T., Ravikrishna, R., McFiggans, G., Mickley, L. J., Martin,
998 S. T., Pöschl, U., Andreae, M. O., and Coe, H.: Enhanced aerosol particle growth sustained by high continental chlorine
999 emission in India, *Nat. Geosci.*, 14, 77–84, <https://doi.org/10.1038/s41561-020-00677-x>, 2021.
- 1000 Guo, H., Liu, J., Froyd, K. D., Roberts, J. M., Veres, P. R., Hayes, P. L., Jimenez, J. L., Nenes, A., and Weber, R. J.: Fine
1001 particle pH and gas-particle phase partitioning of inorganic species in Pasadena, California, during the 2010 CalNex campaign,
1002 *Atmos. Chem. Phys.*, 17, 5703–5719, <https://doi.org/10.5194/acp-17-5703-2017>, 2017.
- 1003 Huang, R. J., Wang, Y., Cao, J., Lin, C., Duan, J., Chen, Q., Li, Y., Gu, Y., Yan, J., Xu, W., Fröhlich, R., Canonaco, F.,
1004 Bozzetti, C., Ovadnevaite, J., Ceburnis, D., Canagaratna, M. R., Jayne, J., Worsnop, D. R., El-Haddad, I., Prevot, A. S. H.,
1005 and O’Dowd, C. D.: Primary emissions versus secondary formation of fine particulate matter in the most polluted city
1006 (Shijiazhuang) in North China, *Atmos. Chem. Phys.*, 19, 2283–2298, <https://doi.org/10.5194/acp-19-2283-2019>, 2019.
- 1007 Jayne, J. T., Leard, D. C., Zhang, X., Davidovits, P., Smith, K. A., Kolb, C. E., and Worsnop, D. R.: Development of an aerosol
1008 mass spectrometer for size and composition analysis of submicron particles, *Aerosol Sci. Technol.*, 33, 49–70,
1009 <https://doi.org/10.1080/027868200410840>, 2000.
- 1010 Jiang, J., Aksoyoglu, S., El-Haddad, I., Ciarelli, G., Denier Van Der Gon, H. A. C., Canonaco, F., Gilardoni, S., Paglione, M.,
1011 Mingüillón, M. C., Favez, O., Zhang, Y., Marchand, N., Hao, L., Virtanen, A., Florou, K., O’Dowd, C., Ovadnevaite, J.,
1012 Baltensperger, U., and Prévôt, A. S. H.: Sources of organic aerosols in Europe: A modeling study using CAMx with modified
1013 volatility basis set scheme, *Atmos. Chem. Phys.*, 19, 15247–15270, <https://doi.org/10.5194/acp-19-15247-2019>, 2019.
- 1014 Jorga, S. D., Florou, K., Kaltsonoudis, C., Kodros, J. K., Vasilakopoulou, C., Cirtog, M., Fouqueau, A., Picquet-Varrault, B.,
1015 Nenes, A., and Pandis, S. N.: Nighttime chemistry of biomass burning emissions in urban areas: A dual mobile chamber study,
1016 *Atmos. Chem. Phys.*, 21, 15337–15349, <https://doi.org/10.5194/acp-21-15337-2021>, 2021.
- 1017 Kadyrov, N., Broquet, G., Chevallier, F., Rivier, L., Gerbig, C., and Ciais, P.: On the potential of the ICOS atmospheric CO₂
1018 measurement network for estimating the biogenic CO₂ budget of Europe, *Atmos. Chem. Phys.*, 15, 12765–12787,
1019 <https://doi.org/10.5194/acp-15-12765-2015>, 2015.
- 1020 Kaltsonoudis, C., Kostenidou, E., Louvaris, E., Psychoudaki, M., Tsiligiannis, E., Florou, K., Liangou, A., and Pandis, S. N.:
1021 Characterization of fresh and aged organic aerosol emissions from meat charbroiling, *Atmos. Chem. Phys.*, 17, 7143–7155,
1022 <https://doi.org/10.5194/acp-17-7143-2017>, 2017.
- 1023 Kleanthous, S., Vrekoussis, M., Mihalopoulos, N., Kalabokas, P., and Lelieveld, J.: On the temporal and spatial variation of
1024 ozone in Cyprus, *Sci. Total Environ.*, 476–477, 677–687, <https://doi.org/10.1016/j.scitotenv.2013.12.101>, 2014.
- 1025 Kodros, J. K., Papanastasiou, D. K., Paglione, M., Masiol, M., Squizzato, S., Florou, K., Skyllakou, K., Kaltsonoudis, C.,
1026 Nenes, A., and Pandis, S. N.: Rapid dark aging of biomass burning as an overlooked source of oxidized organic aerosol, *Proc.*
1027 *Natl. Acad. Sci. U. S. A.*, 117, 33028–33033, <https://doi.org/10.1073/PNAS.2010365117>, 2020.
- 1028 Kostenidou, E., Florou, K., Kaltsonoudis, C., Tsiflikiotou, M., Vratolis, S., Eleftheriadis, K., and Pandis, S. N.: Sources and
1029 chemical characterization of organic aerosol during the summer in the eastern Mediterranean, *Atmos. Chem. Phys.*, 15, 11355–
1030 11371, <https://doi.org/10.5194/acp-15-11355-2015>, 2015.
- 1031 Kushta, J., Georgiou, G. K., Proestos, Y., Christoudias, T., and Lelieveld, J.: Modelling study of the atmospheric composition
1032 over Cyprus, *Atmos. Pollut. Res.*, 9, 257–269, <https://doi.org/10.1016/j.apr.2017.09.007>, 2018.
- 1033 Laborde, M., Crippa, M., Tritscher, T., Jurányi, Z., Decarlo, P. F., Temime-Roussel, B., Marchand, N., Eckhardt, S., Stohl, A.,
1034 Baltensperger, U., Prévôt, A. S. H., Weingartner, E., and Gysel, M.: Black carbon physical properties and mixing state in the
1035 European megacity Paris, *Atmos. Chem. Phys.*, 13, 5831–5856, <https://doi.org/10.5194/acp-13-5831-2013>, 2013.
- 1036 Lanz, V. A., Prévôt, A. S. H., Alfarra, M. R., Weimer, S., Mohr, C., Decarlo, P. F., Gianini, M. F. D., Hueglin, C., Schneider,

- 1037 J., Favez, O., D'Anna, B., George, C., and Baltensperger, U.: Characterization of aerosol chemical composition with aerosol
1038 mass spectrometry in Central Europe: An overview, *Atmos. Chem. Phys.*, 10, 10453–10471, [https://doi.org/10.5194/acp-10-](https://doi.org/10.5194/acp-10-10453-2010)
1039 10453-2010, 2010.
- 1040 Lee, B. H., Kostenidou, E., Hildebrandt, L., Riipinen, I., Engelhart, G. J., Mohr, C., Decarlo, P. F., Mihalopoulos, N., Prevot,
1041 A. S. H., Baltensperger, U., and Pandis, S. N.: Measurement of the ambient organic aerosol volatility distribution: Application
1042 during the Finokalia Aerosol Measurement Experiment (FAME-2008), *Atmos. Chem. Phys.*, 10, 12149–12160,
1043 <https://doi.org/10.5194/acp-10-12149-2010>, 2010.
- 1044 Lelieveld, J., Barlas, C., Giannadaki, D., and Pozzer, A.: Model calculated global, regional and megacity premature mortality
1045 due to air pollution, *Atmos. Chem. Phys.*, 13, 7023–7037, <https://doi.org/10.5194/acp-13-7023-2013>, 2013.
- 1046 Lelieveld, J., Hadjinicolaou, P., Kostopoulou, E., Giannakopoulos, C., Pozzer, A., Tanarhte, M., and Tyrlis, E.: Model
1047 projected heat extremes and air pollution in the eastern Mediterranean and Middle East in the twenty-first century, *Reg.
1048 Environ. Chang.*, 14, 1937–1949, <https://doi.org/10.1007/s10113-013-0444-4>, 2014.
- 1049 Lelieveld, J., Beirle, S., Hörmann, C., Stenchikov, G., and Wagner, T.: Abrupt recent trend changes in atmospheric nitrogen
1050 dioxide over the Middle East, *Sci. Adv.*, 1, 1–6, <https://doi.org/10.1126/sciadv.1500498>, 2015a.
- 1051 Lelieveld, J., Evans, J. S., Fnais, M., Giannadaki, D., and Pozzer, A.: The contribution of outdoor air pollution sources to
1052 premature mortality on a global scale, *Nature*, 525, 367–371, <https://doi.org/10.1038/nature15371>, 2015b.
- 1053 Liu, X., Zheng, M., Liu, Y., Jin, Y., Liu, J., Zhang, B., Yang, X., Wu, Y., Zhang, T., Xiang, Y., Liu, B., and Yan, C.:
1054 Intercomparison of equivalent black carbon (eBC) and elemental carbon (EC) concentrations with three-year continuous
1055 measurement in Beijing, China, *Environ. Res.*, 209, 112791, <https://doi.org/10.1016/j.envres.2022.112791>, 2022.
- 1056 Marmer, E., Dentener, F., V Aardenne, J., Cavalli, F., Vignati, E., Velchev, K., Hjorth, J., Boersma, F., Vinken, G.,
1057 Mihalopoulos, N., and Raes, F.: What can we learn about ship emission inventories from measurements of air pollutants over
1058 the Mediterranean Sea?, *Atmos. Chem. Phys.*, 9, 6815–6831, <https://doi.org/10.5194/acp-9-6815-2009>, 2009.
- 1059 McLinden, C. A., Fioletov, V., Shephard, M. W., Krotkov, N., Li, C., Martin, R. V., Moran, M. D., and Joiner, J.: Space-based
1060 detection of missing sulfur dioxide sources of global air pollution, *Nat. Geosci.*, 9, 496–500, <https://doi.org/10.1038/ngeo2724>,
1061 2016.
- 1062 Michaelides, S., Karacostas, T., Sánchez, J. L., Retalis, A., Pytharoulis, I., Homar, V., Romero, R., Zanis, P., Giannakopoulos,
1063 C., Bühl, J., Ansmann, A., Merino, A., Melcón, P., Lagouvardos, K., Kotroni, V., Bruggeman, A., López-Moreno, J. I., Berthet,
1064 C., Katragkou, E., Tymvios, F., Hadjimitsis, D. G., Mamouri, R. E., and Nisantzi, A.: Reviews and perspectives of high impact
1065 atmospheric processes in the Mediterranean, *Atmos. Res.*, 208, 4–44, <https://doi.org/10.1016/j.atmosres.2017.11.022>, 2018.
- 1066 Middlebrook, A. M., Bahreini, R., Jimenez, J. L., and Canagaratna, M. R.: Evaluation of composition-dependent collection
1067 efficiencies for the Aerodyne aerosol mass spectrometer using field data, *Aerosol Sci. Technol.*, 46, 258–271,
1068 <https://doi.org/10.1080/02786826.2011.620041>, 2012.
- 1069 Middleton, N., Yiallourou, P., Kleanthous, S., Kolokotroni, O., Schwartz, J., Dockery, D. W., Demokritou, P., and Koutrakis,
1070 P.: A 10-year time-series analysis of respiratory and cardiovascular morbidity in Nicosia, Cyprus: The effect of short-term
1071 changes in air pollution and dust storms, *Environ. Heal. A Glob. Access Sci. Source*, 7, 1–16, [https://doi.org/10.1186/1476-](https://doi.org/10.1186/1476-069X-7-39)
1072 069X-7-39, 2008.
- 1073 Mohr, C., DeCarlo, P. F., Heringa, M. F., Chirico, R., Slowik, J. G., Richter, R., Reche, C., Alastuey, A., Querol, X., Seco, R.,
1074 Peñuelas, J., Jiménez, J. L., Crippa, M., Zimmermann, R., Baltensperger, U., and Prévot, A. S. H.: Identification and
1075 quantification of organic aerosol from cooking and other sources in Barcelona using aerosol mass spectrometer data, *Atmos.*
1076 *Chem. Phys.*, 12, 1649–1665, <https://doi.org/10.5194/acp-12-1649-2012>, 2012.
- 1077 Mouzourides, P., Kumar, P., and Neophytou, M. K. A.: Assessment of long-term measurements of particulate matter and
1078 gaseous pollutants in South-East Mediterranean, *Atmos. Environ.*, 107, 148–165,
1079 <https://doi.org/10.1016/j.atmosenv.2015.02.031>, 2015.

- 1080 Neophytou, A. M., Yiallourous, P., Coull, B. A., Kleanthous, S., Pavlou, P., Pashiardis, S., Dockery, D. W., Koutrakis, P., and
 1081 Laden, F.: Particulate matter concentrations during desert dust outbreaks and daily mortality in Nicosia, Cyprus, *J. Expo. Sci.*
 1082 *Environ. Epidemiol.*, 23, 275–280, <https://doi.org/10.1038/jes.2013.10>, 2013.
- 1083 Ng, N. L., Canagaratna, M. R., Jimenez, J. L., Zhang, Q., Ulbrich, I. M., and Worsnop, D. R.: Real-time methods for estimating
 1084 organic component mass concentrations from aerosol mass spectrometer data, *Environ. Sci. Technol.*, 45, 910–916,
 1085 <https://doi.org/10.1021/es102951k>, 2011.
- 1086 Olivier, J. G. J., Van Aardenne, J. A., Dentener, F. J., Pagliari, V., Ganzeveld, L. N., and Peters, J. A. H. W.: Recent trends in
 1087 global greenhouse gas emissions: regional trends 1970–2000 and spatial distribution of key sources in 2000, *Environ. Sci.*, 2,
 1088 81–99, <https://doi.org/10.1080/15693430500400345>, 2005.
- 1089 Osipov, S., Chowdhury, S., Crowley, J. N., Tadic, I., Drewnick, F., Borrmann, S., Eger, P., Fachinger, F., Fischer, H.,
 1090 Predybaylo, E., Fnais, M., Harder, H., Pikridas, M., Vouterakos, P., Pozzer, A., Sciare, J., Ukhov, A., Stenchikov, G. L.,
 1091 Williams, J., and Lelieveld, J.: Severe atmospheric pollution in the Middle East is attributable to anthropogenic sources,
 1092 *Commun. Earth Environ.*, 3, 1–10, <https://doi.org/10.1038/s43247-022-00514-6>, 2022.
- 1093 Paatero, P.: The Multilinear Engine—A Table-Driven, Least Squares Program for Solving Multilinear Problems, Including
 1094 the n-Way Parallel Factor Analysis Model, *J. Comput. Graph. Stat.*, 8, 854–888,
 1095 <https://doi.org/10.1080/10618600.1999.10474853>, 1999.
- 1096 Paatero, P. and Hopke, P. K.: Discarding or downweighting high-noise variables in factor analytic models, *Anal. Chim. Acta*,
 1097 490, 277–289, [https://doi.org/10.1016/S0003-2670\(02\)01643-4](https://doi.org/10.1016/S0003-2670(02)01643-4), 2003.
- 1098 Paatero, P. and Hopke, P. K.: Rotational tools for factor analytic models, *J. Chemom.*, 23, 91–100,
 1099 <https://doi.org/10.1002/cem.1197>, 2009.
- 1100 Paris, J. D., Riandet, A., Bourtsoukidis, E., Delmotte, M., Berchet, A., Williams, J., Ernle, L., Tadic, I., Harder, H., and
 1101 Lelieveld, J.: Shipborne measurements of methane and carbon dioxide in the Middle East and Mediterranean areas and the
 1102 contribution from oil and gas emissions, *Atmos. Chem. Phys.*, 21, 12443–12462, <https://doi.org/10.5194/acp-21-12443-2021>,
 1103 2021.
- 1104 Petit, J. E., Favez, O., Sciare, J., Crenn, V., Sarda-Estève, R., Bonnaire, N., Močnik, G., Dupont, J. C., Haeffelin, M., and
 1105 Leoz-Garziandia, E.: Two years of near real-time chemical composition of submicron aerosols in the region of Paris using an
 1106 Aerosol Chemical Speciation Monitor (ACSM) and a multi-wavelength Aethalometer, *Atmos. Chem. Phys.*, 15, 2985–3005,
 1107 <https://doi.org/10.5194/acp-15-2985-2015>, 2015.
- 1108 Petit, J. E., Favez, O., Albinet, A., and Canonaco, F.: A user-friendly tool for comprehensive evaluation of the geographical
 1109 origins of atmospheric pollution: Wind and trajectory analyses, *Environ. Model. Softw.*, 88, 183–187,
 1110 <https://doi.org/10.1016/j.envsoft.2016.11.022>, 2017.
- 1111 Pey, J., Querol, X., Alastuey, A., Forastiere, F., and Stafoggia, M.: African dust outbreaks over the Mediterranean Basin during
 1112 2001–2011: PM10 concentrations, phenomenology and trends, and its relation with synoptic and mesoscale meteorology,
 1113 *Atmos. Chem. Phys.*, 13, 1395–1410, <https://doi.org/10.5194/acp-13-1395-2013>, 2013.
- 1114 Pikridas, M., Vrekoussis, M., Sciare, J., Kleanthous, S., Vasiliadou, E., Kizas, C., Savvides, C., and Mihalopoulos, N.: Spatial
 1115 and temporal (short and long-term) variability of submicron, fine and sub-10 Mm particulate matter (PM1, PM2.5, PM10) in
 1116 Cyprus, *Atmos. Environ.*, 191, 79–93, <https://doi.org/10.1016/j.atmosenv.2018.07.048>, 2018.
- 1117 Poulain, L., Fahlbusch, B., Spindler, G., Müller, K., Van Pinxteren, D., Wu, Z., Iinuma, Y., Birmili, W., Wiedensohler, A.,
 1118 and Herrmann, H.: Source apportionment and impact of long-range transport on carbonaceous aerosol particles in central
 1119 Germany during HCCT-2010, *Atmos. Chem. Phys.*, 21, 3667–3684, <https://doi.org/10.5194/acp-21-3667-2021>, 2021.
- 1120 Pozzer, A., Zimmermann, P., Doering, U. M., Van Aardenne, J., Tost, H., Dentener, F., Janssens-Maenhout, G., and Lelieveld,
 1121 J.: Effects of business-as-usual anthropogenic emissions on air quality, *Atmos. Chem. Phys.*, 12, 6915–6937,
 1122 <https://doi.org/10.5194/acp-12-6915-2012>, 2012.

- 1123 Querol, X., Pey, J., Pandolfi, M., Alastuey, A., Cusack, M., Pérez, N., Moreno, T., Viana, M., Mihalopoulos, N., Kallos, G.,
 1124 and Kleanthous, S.: African dust contributions to mean ambient PM10 mass-levels across the Mediterranean Basin, *Atmos.*
 1125 *Environ.*, 43, 4266–4277, <https://doi.org/10.1016/j.atmosenv.2009.06.013>, 2009.
- 1126 Rattanavaraha, W., Canagaratna, M. R., Budisulistiorini, S. H., Croteau, P. L., Baumann, K., Canonaco, F., Prevot, A. S. H.,
 1127 Edgerton, E. S., Zhang, Z., Jayne, J. T., Worsnop, D. R., Gold, A., Shaw, S. L., and Surratt, J. D.: Source apportionment of
 1128 submicron organic aerosol collected from Atlanta, Georgia, during 2014–2015 using the aerosol chemical speciation monitor
 1129 (ACSM), *Atmos. Environ.*, 167, 389–402, <https://doi.org/10.1016/j.atmosenv.2017.07.055>, 2017.
- 1130 Ricaud, P., Zbinden, R., Catoire, V., Brocchi, V., Dulac, F., Hamonou, E., Canonici, J. C., El Amraoui, L., Massart, S., Piguet,
 1131 B., Dayan, U., Nabat, P., Sciare, J., Ramonet, M., Delmotte, M., Di Sarra, A., Sferlazzo, D., Di Iorio, T., Piacentino, S.,
 1132 Cristofanelli, P., Mihalopoulos, N., Kouvarakis, G., Pikridas, M., Savvides, C., Mamouri, R. E., Nisantzi, A., Hadjimitsis, D.,
 1133 Attié, J. L., Ferré, H., Kangah, Y., Jaidan, N., Guth, J., Jacquet, P., Chevrier, S., Robert, C., Bourdon, A., Bourdinot, J. F.,
 1134 Etienne, J. C., Krysztofiak, G., and Theron, P.: The GLAM airborne campaign across the Mediterranean Basin, *Bull. Am.*
 1135 *Meteorol. Soc.*, 99, 361–380, <https://doi.org/10.1175/BAMS-D-16-0226.1>, 2018.
- 1136 Rigler, M., Drinovec, L., Lavri, G., Vlachou, A., Prevot, A. S. H., Luc Jaffrezo, J., Stavroulas, I., Sciare, J., Burger, J., Kranjc,
 1137 I., Turšič, J., D. A. Hansen, A., and Mocnik, G.: The new instrument using a TC-BC (total carbon-black carbon) method for
 1138 the online measurement of carbonaceous aerosols, *Atmos. Meas. Tech.*, 13, 4333–4351, [https://doi.org/10.5194/amt-13-4333-](https://doi.org/10.5194/amt-13-4333-2020)
 1139 2020, 2020.
- 1140 Sandradewi, J., Prévôt, A. S. H., Szidat, S., Perron, N., Alfarra, M. R., Lanz, V. A., Weingartner, E., and Baltensperger, U. R.
 1141 S.: Using aerosol light absorption measurements for the quantitative determination of wood burning and traffic emission
 1142 contribution to particulate matter, *Environ. Sci. Technol.*, 42, 3316–3323, <https://doi.org/10.1021/es702253m>, 2008.
- 1143 Sciare, J., Bardouki, H., Moulin, C., and Mihalopoulos, N.: Aerosol sources and their Contribution to the chemical composition
 1144 of aerosols in the Eastern Mediterranean Sea during summertime, *Atmos. Chem. Phys.*, 3, 291–302,
 1145 <https://doi.org/10.5194/acp-3-291-2003>, 2003.
- 1146 Sciare, J., D'Argouges, O., Zhang, Q. J., Sarda-Estève, R., Gaimoz, C., Gros, V., Beekmann, M., and Sanchez, O.: Comparison
 1147 between simulated and observed chemical composition of fine aerosols in Paris (France) during springtime: Contribution of
 1148 regional versus continental emissions, *Atmos. Chem. Phys.*, 10, 11987–12004, <https://doi.org/10.5194/acp-10-11987-2010>,
 1149 2010.
- 1150 Siouti, E., Skyllakou, K., Kioutsioukis, I., Ciarelli, G., and Pandis, S. N.: Simulation of the cooking organic aerosol
 1151 concentration variability in an urban area, *Atmos. Environ.*, 265, 118710, <https://doi.org/10.1016/j.atmosenv.2021.118710>,
 1152 2021.
- 1153 Smith, S. J., Van Aardenne, J., Klimont, Z., Andres, R. J., Volke, A., and Delgado Arias, S.: Anthropogenic sulfur dioxide
 1154 emissions: 1850–2005, *Atmos. Chem. Phys.*, 11, 1101–1116, <https://doi.org/10.5194/acp-11-1101-2011>, 2011.
- 1155 Stavroulas, I., Bougiatioti, A., Grivas, G., Paraskevopoulou, D., Tsagkaraki, M., Zarmas, P., Liakakou, E., Gerasopoulos, E.,
 1156 and Mihalopoulos, N.: Sources and processes that control the submicron organic aerosol composition in an urban
 1157 Mediterranean environment (Athens): A high temporal-resolution chemical composition measurement study, *Atmos. Chem.*
 1158 *Phys.*, 19, 901–919, <https://doi.org/10.5194/acp-19-901-2019>, 2019.
- 1159 Stavroulas, I., Grivas, G., Liakakou, E., Kalkavouras, P., Bougiatioti, A., Kaskaoutis, D. G., Lianou, M., Papoutsidaki, K.,
 1160 Tsagkaraki, M., Zarmas, P., Gerasopoulos, E., and Mihalopoulos, N.: Online chemical characterization and sources of
 1161 submicron aerosol in the major mediterranean port city of piraeus, greece, *Atmosphere (Basel)*, 12, 1–28,
 1162 <https://doi.org/10.3390/atmos12121686>, 2021.
- 1163 Stein, A. F., Draxler, R. R., Rolph, G. D., Stunder, B. J. B., Cohen, M. D., and Ngan, F.: NOAA's hysplit atmospheric transport
 1164 and dispersion modeling system, *Bull. Am. Meteorol. Soc.*, 96, 2059–2077, <https://doi.org/10.1175/BAMS-D-14-00110.1>,
 1165 2015.
- 1166 Sun, C., Lee, B. P., Huang, D., Jie Li, Y., Schurman, M. I., Louie, P. K. K., Luk, C., and Chan, C. K.: Continuous measurements
 1167 at the urban roadside in an Asian megacity by Aerosol Chemical Speciation Monitor (ACSM): Particulate matter characteristics
 1168 during fall and winter seasons in Hong Kong, *Atmos. Chem. Phys.*, 16, 1713–1728, <https://doi.org/10.5194/acp-16-1713-2016>,

1169 2016.

1170 Terink, W., Immerzeel, W. W., and Droogers, P.: Climate change projections of precipitation and reference evapotranspiration
1171 for the Middle East and Northern Africa until 2050, *Int. J. Climatol.*, 33, 3055–3072, <https://doi.org/10.1002/joc.3650>, 2013.

1172 Theodosi, C., Grivas, G., Zarmas, P., Chaloulakou, A., and Mihalopoulos, N.: Mass and chemical composition of size-
1173 segregated aerosols (PM₁, PM_{2.5}, PM₁₀) over Athens, Greece: Local versus regional sources, *Atmos. Chem. Phys.*, 11,
1174 11895–11911, <https://doi.org/10.5194/acp-11-11895-2011>, 2011.

1175 Theodosi, C., Tsagkaraki, M., Zarmas, P., Grivas, G., Liakakou, E., Paraskevopoulou, D., Lianou, M., Gerasopoulos, E., and
1176 Mihalopoulos, N.: Multi-year chemical composition of the fine-aerosol fraction in Athens, Greece, with emphasis on the
1177 contribution of residential heating in wintertime, *Atmos. Chem. Phys.*, 18, 14371–14391, <https://doi.org/10.5194/acp-18-14371-2018>, 2018.

1179 Trubetskaya, A., Lin, C., Ovadnevaite, J., Ceburnis, D., O’Dowd, C., Leahy, J. J., Monaghan, R. F. D., Johnson, R., Layden,
1180 P., and Smith, W.: Study of Emissions from Domestic Solid-Fuel Stove Combustion in Ireland, *Energy and Fuels*, 35, 4966–
1181 4978, <https://doi.org/10.1021/acs.energyfuels.0c04148>, 2021.

1182 Tsangari, H., Paschalidou, A. K., Kassomenos, A. P., Vardoulakis, S., Heaviside, C., Georgiou, K. E., and Yamasaki, E. N.:
1183 Extreme weather and air pollution effects on cardiovascular and respiratory hospital admissions in Cyprus, *Sci. Total Environ.*,
1184 542, 247–253, <https://doi.org/10.1016/j.scitotenv.2015.10.106>, 2016.

1185 Tuccella, P., Curci, G., Visconti, G., Bessagnet, B., Menut, L., and Park, R. J.: Modeling of gas and aerosol with WRF/Chem
1186 over Europe: Evaluation and sensitivity study, *J. Geophys. Res. Atmos.*, 117, 1–15, <https://doi.org/10.1029/2011JD016302>,
1187 2012.

1188 Ulbrich, I. M., Canagaratna, M. R., Zhang, Q., Worsnop, D. R., and Jimenez, J. L.: Interpretation of organic components from
1189 Positive Matrix Factorization of aerosol mass spectrometric data, *Atmos. Chem. Phys.*, 9, 2891–2918,
1190 <https://doi.org/10.5194/acp-9-2891-2009>, 2009.

1191 Vrekoussis, M., Pikridas, M., Rousogenous, C., Christodoulou, A., Desservettaz, M., Sciare, J., Richter, A., Bougoudis, I.,
1192 Savvides, C., and Papadopoulos, C.: Local and regional air pollution characteristics in Cyprus: A long-term trace gases
1193 observations analysis, *Sci. Total Environ.*, 845, 157315, <https://doi.org/10.1016/j.scitotenv.2022.157315>, 2022.

1194 Xu, W., He, Y., Qiu, Y., Chen, C., Xie, C., Lei, L., Li, Z., Sun, J., Li, J., Fu, P., Wang, Z., Worsnop, D. R., and Sun, Y.: Mass
1195 spectral characterization of primary emissions and implications in source apportionment of organic aerosol, *Atmos. Meas.*
1196 *Tech.*, 13, 3205–3219, <https://doi.org/10.5194/amt-13-3205-2020>, 2020.

1197 Zanis, P., Hadjinicolaou, P., Pozzer, A., Tyrllis, E., Dafka, S., Mihalopoulos, N., and Lelieveld, J.: Summertime free-
1198 tropospheric ozone pool over the eastern Mediterranean/middle east, *Atmos. Chem. Phys.*, 14, 115–132,
1199 <https://doi.org/10.5194/acp-14-115-2014>, 2014.

1200 Zhang, Y., Favez, O., Canonaco, F., Liu, D., Močnik, G., Amodeo, T., Sciare, J., Prévôt, A. S. H., Gros, V., and Albinet, A.:
1201 Evidence of major secondary organic aerosol contribution to lensing effect black carbon absorption enhancement, *npj Clim.*
1202 *Atmos. Sci.*, 1, <https://doi.org/10.1038/s41612-018-0056-2>, 2018.

1203 Zhang, Y., Favez, O., Petit, J. E., Canonaco, F., Truong, F., Bonnaire, N., Crenn, V., Amodeo, T., Prévôt, A. S. H., Sciare, J.,
1204 Gros, V., and Albinet, A.: Six-year source apportionment of submicron organic aerosols from near-continuous highly time-
1205 resolved measurements at SIRTa (Paris area, France), *Atmos. Chem. Phys.*, 19, 14755–14776, <https://doi.org/10.5194/acp-19-14755-2019>, 2019.

1207 Zittis, G., Almazroui, M., Alpert, P., Ciais, P., Cramer, W., Dahdal, Y., Fnais, M., Francis, D., Hadjinicolaou, P., Howari, F.,
1208 Jrrar, A., Kaskaoutis, D. G., Kulmala, M., Lazoglou, G., Mihalopoulos, N., Lin, X., Rudich, Y., Sciare, J., Stenchikov, G.,
1209 Xoplaki, E., and Lelieveld, J.: Climate Change and Weather Extremes in the Eastern Mediterranean and Middle East, *Rev.*
1210 *Geophys.*, 60, <https://doi.org/10.1029/2021rg000762>, 2022.

1211